Monthly Notices
of the
ROYAL ASTRONOMICAL SOCIETY

MNRAS **550**, 1–25 (2026)
Advance Access publication 2026 July 10

https://doi.org/10.1093/mnras/stag1305

Planetary systems in the light of asteroseismology: metallicity threshold for the planetary systems and age–metallicity relation

M. Yıldız [1]★ A. Demirkol,[2] S. Örtel [2] T. Çakır Alsaç [2] and T. Daylan[3]

[1]Department of Astronomy and Space Sciences, Faculty of Science, Ege University, 35100 İzmir, Turkey
[2]Department of Astronomy and Space Sciences, Graduate School of Natural and Applied Sciences, Ege University, 35100 İzmir, Turkey
[3]Department of Physics, Washington University, St. Louis, MO 63130, USA

Accepted 2026 July 7. Received 2026 July 7; in original form 2025 November 3

ABSTRACT

We compiled data for 127 hosts (plus six candidates) and used them as constraints to construct interior models of the hosts using the MESA code. Two significant conclusions emerge from these models. First, except for a few stars, the hosts' metallicity (Z_0) is greater than 0.007. This suggests a possible suppression of the occurrence of planets below $Z_0 \approx 0.007$. Second, it concerns how chemical evolution unfolds in the galactic disc. For a given Z_0 value, considering the oldest stars, there is a linear relationship between Z_0 and age (t_9). This line is around t_9=13.4 Gyr at Z_0=0, a value consistent with the age of the Galaxy. The linear relationship continues until around t_9=6 Gyr, and the maximum value of Z_0 remains constant between t_9=2–6 Gyr. We further modelled 12 hosts classified as red clump (RC) stars in the literature, explicitly accounting for mass-loss along the red giant branch. These models highlight the critical role of mass-loss assumptions in determining the initial masses and ages of RC hosts, and their implications for the survival and evolution of close-in planets. Another key outcome of this study is the discovery of the relationship between Z_0 and the observed metallicity (Z_s) for the hosts. We obtain a useful expression for Z_0, the input parameter for the models, as a function of stellar mass, radius, and Z_s. This expression can be used to estimate Z_0 based on the reduced surface metallicity due to microscopic diffusion. We also derive an expression for planetary mass relative to the orbital semimajor axis and host mass. This expression may indicate a mass distribution near the inner disc where these planets formed, except for hot-Jupiters. Planet radii appear to depend on the planet's mass and irradiation energy, as well as the orbital period.

Key words: planets and satellites: formation – planets and satellites: general – stars: evolution – stars: interior – stars: oscillation – planetary systems.

1 INTRODUCTION

Understanding and modeling the internal structures of stars is crucial to astrophysics. Although traditional methods like spectroscopy and photometry provide valuable insights into stars, they become less effective as we probe deeper into a star's interior. This is where asteroseismology emerges as a revolutionary technique. Asteroseismology, the study of seismic waves within stars, has become an essential tool in astrophysics, providing invaluable knowledge of stellar dynamics. Many stars display oscillatory behaviour. These oscillations lead to periodic variations in brightness as they expand and contract. For Sun and solar-like stars, oscillations are driven by convective processes that occur in their outer layers.

Fortunately, solar-like oscillations have been detected in many host stars, primarily from the light curves provided by recent space missions such as ESA's Convection, Rotation, and planetary Transits (CoRoT; A. Baglin et al. 2006), NASA's Kepler/K2 (W. J. Borucki et al. 2010b; S. B. Howell et al. 2014), and the Transiting Exoplanet Survey Satellite (TESS; G. R. Ricker et al. 2015). These missions have provided high-quality data for both asteroseismology and exoplanet science, greatly strengthening the connection between the two fields and allowing them to advance together (V. Van Eylen et al. 2015; D. Huber 2016). Asteroseismology provides precise constraints on the internal structure and evolutionary state of stars, which are essential for the characterization of planetary systems (D. Huber et al. 2013a; V. Silva Aguirre et al. 2015). Fundamental characteristics of exoplanets, such as their mass, radius, age, and atmospheric composition, critically depend on the accuracy of the host star parameters. The more accurately we can determine the properties of the host star, the better we can assess the parameters of the orbiting planets.

In this study, we compiled asteroseismic and non-asteroseismic data of 133 solar-like oscillating stars and their planets from the literature. 6 of them are planet candidate systems (KOI-5/KIC 8554498, KOI-75/KIC 7199397, KOI-268/KIC 3425851, KOI-364/KIC 7296438, KOI-974/KIC 9414417, and KOI-2640/KIC 9088780). We did not remove these stars, but we listed them separately. We examine how asteroseismology plays a key role in

★ E-mail: mutlu.yildiz@ege.edu.tr

studying planetary systems and its importance in enhancing our understanding of these stars. Similar studies are available in the literature (D. Huber et al. 2013a; C. Kayhan, M. Yıldız & Z. Çelik Orhan 2019). These studies are based on a detailed modelling of the hosts and host candidates.

At the beginning of this study, approximately 40 hosts were compiled from the literature. With newly published studies, this number first increased to 80, and then to 127. A recent study by W.-X. Lin et al. (2025b) lists asteroseismic data for 142 hosts and computes fundamental properties of hosts and then planets using the asteroseismic scaling relations. Because the updates are endless, we had to stop at some point. 97 of the 142 hosts are available in our catalogue. In a similar study, M. Sayeed et al. (2025) compiled an asteroseismic catalogue of 765 Kepler main-sequence (MS) and subgiant (SG) stars. Their analysis revealed 50 new detections, including seven planet candidate host stars. The catalogue includes 101 stars with planets. 38 of these stars are available in our catalogue.

The hosts in which planetary systems form and the extent to which planets' properties depend on their host mass, for example, are key questions. How planets evolve, both structurally and orbitally, is also a key question to answer.

In particular, determining planetary radii with high precision is of great importance. One of the main reasons for this is that the radius is the parameter that best represents the structure and evolution of planets compared to stars. After a planet forms, it cools relatively rapidly, reducing its radius. Planets with the biggest radii are those exposed to high irradiation (gas giants) (A. Burrows et al. 2000; E. D. Lopez & J. J. Fortney 2016). Whether these planets cool over time can be understood from the change in their radius. Therefore, understanding how irradiation affects planetary evolution depends on accurately determining planetary radii. Moreover, even small uncertainties in the stellar radius can significantly affect the estimated planetary radius and, indirectly, our interpretation of the planet's composition (M. S. Lundkvist et al. 2018). Thanks to asteroseismology, stellar radii can be determined with remarkable precision, thereby overcoming this issue.

Equally importantly, the age of the system plays a key role, as it reveals how these planets have evolved over time. Since age is not directly observable, it remains difficult to constrain. Assuming that planets and their host stars form simultaneously, the planetary age can be inferred from the stellar age. The age of a planetary system provides important insight into the dynamical processes responsible for shaping the current structure of planetary systems, such as migration and star–planet interaction. It also plays a key role in the development of search strategies for potentially habitable planets (M. Safonova, J. Murthy & Y. A. Shchekinov 2016). In this study, we compiled 127 planet-host stars (along with six candidates) from the literature and constructed interior models with MESA (B. Paxton et al. 2011, 2013, 2015, 2018, 2019; A. S. Jermyn et al. 2023).

The study of planet-host stars that exhibit asteroseismic oscillations is fundamental for future stellar and exoplanet research. The primary aim of this study is to investigate planetary systems as a whole using asteroseismic data and to derive stellar and planetary parameters with higher reliability compared to other available methods. In this context, the study is intended to serve as a solid reference for the investigation of planetary systems and to support future research by addressing a wide range of questions related to both stars and their planets.

The paper is organized as follows: Section 2 presents the observed properties of the host stars and their planetary systems, together with the asteroseismic scaling relations. Section 3 describes the modelling methodology adopted in this study. The results of the computations are presented and discussed in Section 4. Finally, Section 5 provides the main conclusions of this study.

2 ASTEROSEISMIC AND NON-ASTEROSEISMIC OBSERVED PROPERTIES OF PLANET HOSTS AND ASTEROSEISMIC SCALING RELATIONS BETWEEN THEM

The search for life on planets other than Earth, a highly popular field of research today, has led to a much more detailed study of planetary systems. In this study, knowledge of host stars, in particular, facilitates the study of planets. Accurate determination of stellar parameters such as radius, mass, age, and metallicity enables planetary radius and mass (see Table A2) with comparable accuracy. This is because indirect detection methods such as the transit and radial velocity techniques derive planetary properties through their host stars. In the transit method, the planet-to-star radius ratio is measured from the transit depth, making the planetary radius directly proportional to the stellar radius. Similarly, radial velocity observations yield the planetary mass relative to the stellar mass, so the inferred planetary mass depends on the adopted stellar mass. Consequently, uncertainties in stellar parameters propagate directly into the derived planetary properties (D. Huber 2018). For this reason, asteroseismology, the most effective method for explaining the internal structure and evolution of stars, has become an essential tool in the study of planetary systems. We compiled asteroseismic and spectroscopic data of systems containing planets from the literature (Table A1).

2.1 Asteroseismic scaling relations

Two fundamental asteroseismic quantities are significant: the value of the large frequency separation between oscillation frequencies ($\Delta\nu$), and the frequency of maximum amplitude ($\nu_{\rm max}$). $\Delta\nu$ is defined as the frequency difference between modes of equal spherical degree ℓ, and consecutive radial orders n. This quantity is intrinsically linked to the acoustic travel time within the star and is approximately proportional to the square root of the mean stellar density ($\bar{\rho}$) (M. Tassoul 1980; J. Christensen-Dalsgaard 1993). $\nu_{\rm max}$ scales approximately as $g/\sqrt{T_{\rm eff}}$, where g is the surface gravity (T. M. Brown et al. 1991; H. Kjeldsen & T. R. Bedding 1995). As stars evolve and surface gravity decreases, $\nu_{\rm max}$ shifts toward lower frequencies.

The mean of $\Delta\nu$ ($\langle\Delta\nu\rangle$) and $\nu_{\rm max}$ play an important role in determining the mass (M) and radius (R) of oscillating stars. The standard asteroseismic scaling relations, which allow the estimation of the radius ($R_{\rm sca}$) and mass ($M_{\rm sca}$) of an oscillating star, are given as follows:

$$\frac{R_{\rm sca}}{\rm R_{\odot}} = \frac{\nu_{\rm max}/\nu_{\rm max\odot}}{(\langle\Delta\nu\rangle\,/\,\langle\Delta\nu_{\odot}\rangle)^2}\left(\frac{T_{\rm eff}}{\rm T_{eff\odot}}\right)^{1/2}, \quad (1)$$

$$\frac{M_{\rm sca}}{\rm M_{\odot}} = \frac{(\nu_{\rm max}/\nu_{\rm max\odot})^3}{(\langle\Delta\nu\rangle\,/\,\langle\Delta\nu_{\odot}\rangle)^4}\left(\frac{T_{\rm eff}}{\rm T_{eff\odot}}\right)^{3/2}. \quad (2)$$

Here, $\langle\Delta\nu_{\odot}\rangle$ and $\nu_{\rm max\odot}$ correspond to the solar values and the adopted values of $\langle\Delta\nu_{\odot}\rangle = 135.1\ \mu$Hz and $\nu_{\rm max\odot} = 3090\ \mu$Hz (S. Sharma et al. 2016).

The small frequency separation ($\delta\nu$) is another crucial asteroseismic parameter (J. Christensen-Dalsgaard 1988). It is defined as the frequency difference between modes of consecutive radial order n and with a degree difference of two. The $\delta\nu_{02}$, calculated from modes with $l = 0$ and $l = 2$, is highly sensitive to the conditions in the stellar core during the MS, making it a valuable age indicator. As a star evolves along the MS, $\delta\nu_{02}$ decreases, being about 15 μHz at the zero-age main sequence (ZAMS) and around 5 μHz near the terminal-age main sequence (TAMS). For the Sun, $\delta\nu_{02}$ has a value of 9.8 μHz (M. Yıldız, Z. Çelik Orhan & C. Kayhan 2016), which indicates that it is roughly halfway through its MS lifetime.

In this study, we analyse host stars at different evolutionary stages. Only a few of the solar-like oscillating host stars in the literature are MS stars. The vast majority are SG and red giant branch (RGB) or red clump (RC) stars. Both the different structures of stars at different evolutionary stages and the fact that non-asteroseismic observational data, especially, have different uncertainty levels prevent us from applying a single modelling method. Therefore, it would be more useful to apply the technique based on each star's observational data. We used $\Delta\nu$ and surface metallicity (Z_s) constraints for each star. We also used the reference frequencies ($\nu_{\rm min0}$ and $\nu_{\rm min1}$), effective temperature ($T_{\rm eff}$), luminosity (L), and R calculated from the scaling relations as constraints according to the uncertainty level in the data of the stars. Analyzing the results obtained by applying several methods to some hosts would help us decide which method we prefer.

Detailed models of host stars are essential for many reasons: (i) good determination of the mass and radius of the stars allows good determination of the mass (M_p) and radius (R_p) of the transiting planets, (ii) the initial chemical composition of the star affects its own structure and also represents the chemical composition of the environment in which the planet formed, (iii) the age, which we can determine more precisely, especially with asteroseismic data, also reveals how the planets have evolved from the time they formed to the present.

2.2 Non-asteroseismic properties of the planetary systems

The luminosities of the stars in Table A1 are primarily obtained from references using GAIA DR3 and DR2 data (Gaia Collaboration 2018, 2021). Many studies provide observed metallicity ([M/H]) and $T_{\rm eff}$ values for many of the hosts. Generally, these values are quite scattered. In this case, we tried to construct interior models for a host and obtain the observational data that best fit its model. The Hertzsprung–Russell diagram (HRD) plotted from the compiled data is shown in Fig. 1. According to the TAMS line (M. Yıldız 2015), around 15 planet hosts are MS stars. Nearly 25 hosts are SGs, and the remaining hosts are RGB or RC stars. There may be a small number of core-helium-burning (CHeB) stars among the stars in the red giant (RG). Masses of the hosts range from 0.76 to 2.66 $M_\odot$. The radius interval is about 0.75–16.21 $R_\odot$.

[M/H] (or [Fe/H]) and $T_{\rm eff}$ of the hosts are adopted from the spectroscopic studies in the literature (see Table A1). [M/H] represents the metallicity of the photosphere of the hosts. For the interior models, however, the initial metallicity (Z_0) is the input parameter. For the evolved stars, Z_0 can be taken as Z_s. However, for the hosts on and around MS, Z_s may significantly be less than Z_0, due to microscopic diffusion, depending on the age and depth of the stellar convective envelope. The Z_s of the planet hosts are computed from the [M/H] values:

$$Z_s = 10^{[{\rm M/H}]} Z_\odot,$$

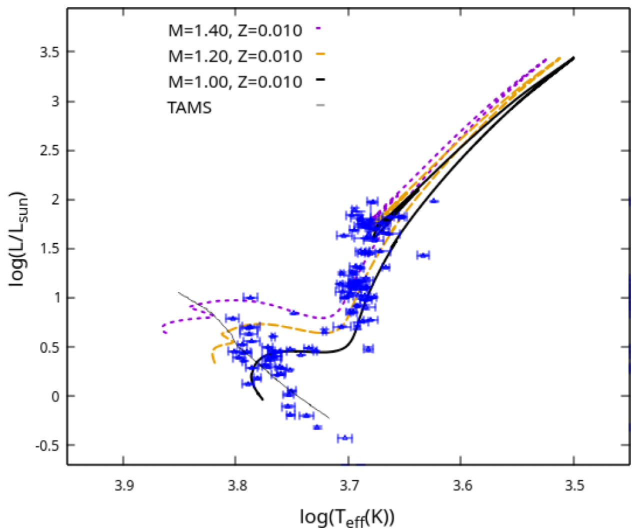

Figure 1. The classical HRD of the oscillating host stars. The thick solid and dashed lines represent the evolutionary tracks at $Z = 0.0100$ for 1.0, 1.2, and 1.4 $M_\odot$. The thin solid line denotes the TAMS.

where $Z_\odot$ is the solar metallicity and taken as 0.0134 (M. Asplund et al. 2009). For two of the hosts, namely KIC 6278762 and TIC 160224839, Z_s is small, $\sim$ 0.006. For most of the stars, [M/H] ranges from −0.3 to 0.3 dex. This implies that [M/H] for most of the systems varies between 0.007 and 0.027.

As part of our study, we examined 133 planetary systems. We compiled the masses, radii, orbital periods, and semimajor axis lengths of the planets from the literature to create a catalogue. The references for the planetary parameters in Table A1 are marked in bold for clarity. In our sample, planetary masses range from 22.900 M_J to 0.0076 M_J, while radii span 1.36 R_J to 0.027 R_J. A total of 27 multiplanet systems are identified. Since asteroseismology allows us to determine the fundamental parameters of host stars with high precision, the properties of their planets can also be constrained with great accuracy. Therefore, these systems are of particular importance for studying planetary evolution and characterizing their fundamental properties (see Sections 4.9 and 4.10).

2.3 Asteroseismic properties of the hosts

The asteroseismic properties of the majority of planet hosts have been published in several studies (T. Appourchaux et al. 2012; D. Huber et al. 2013a; V. Silva Aguirre et al. 2015; G. R. Davies et al. 2016; C. Kayhan et al. 2019; J. Zhou et al. 2024). The quality of observational data of each planetary system and the number of observables are quite different from the others. While for some stars the available asteroseismic data include only their $\Delta\nu$, some of them have individual oscillation frequencies for many modes. Determining many oscillation frequencies is important because we can then use the reference frequencies as constraints. The asteroseismic properties of the Kepler RC and RGB targets are given in the APOKASC-2 catalogues. $\nu_{\rm max}$ and $\Delta\nu$ of the TESS targets are mainly published in references. $\nu_{\rm max}$ of the hosts is plotted with respect to $\Delta\nu$ in Fig. 2(a). $\Delta\nu$ of RC and RGB stars ranges 2.5–8.8 and 0.45–18.7 μHz, respectively. $\nu_{\rm max}$ of RC and RGB stars range 18.6–115 and 2.02–246.7 μHz, respectively. The masses of the stars in the APOKASC-2 catalogue range between

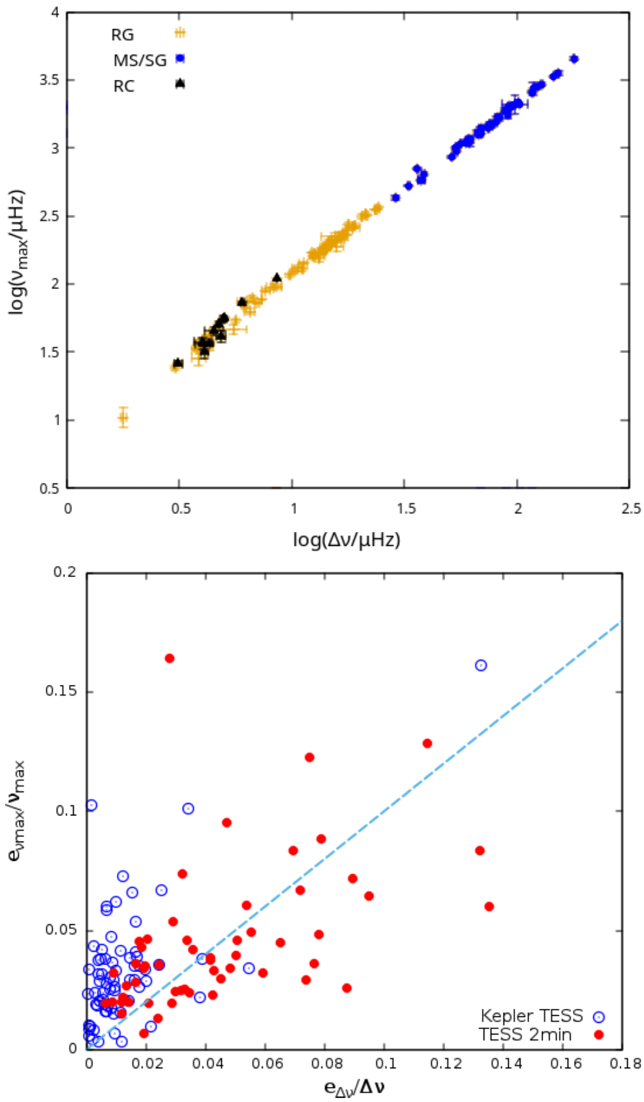

Figure 2. (a) $\nu_{\max}$ is plotted with respect to $\Delta\nu$ in logarithmic scales. The cross, filled circle, and triangle are for RG, MS/SG, and RC stars, respectively. (b) Uncertainty of $\nu_{\max}$ is plotted with respect to $\Delta\nu$.

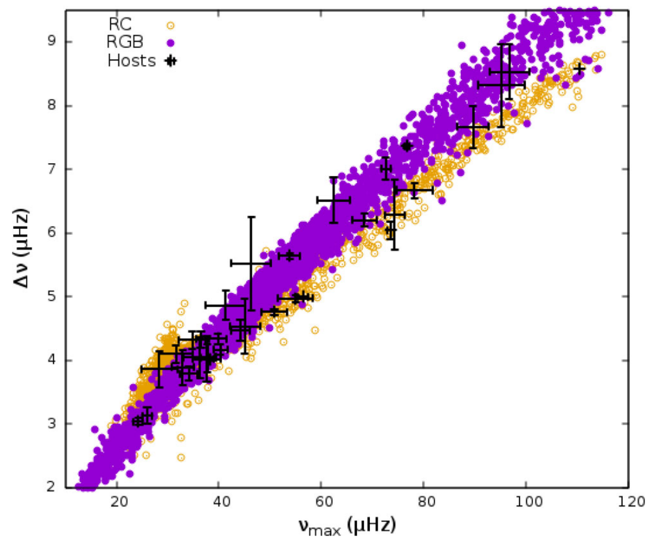

Figure 3. $\Delta\nu$ is plotted with respect to $\nu_{\max}$ for hosts to compare with RGB and RC stars in APOKASC-2. In this diagram, RC and RGB stars are slightly separated. Some of the hosts are likely RC stars.

0.8 and 2.5 $M_\odot$ with a peak at around 1.2 $M_\odot$. The stellar radii span from 2 to 40 $R_\odot$.

Fig. 2(b) shows the relative uncertainty of $\nu_{\max}$ ($e_{\nu_{\max}}/\nu_{\max}$) plotted against the relative uncertainty of $\Delta\nu$ ($e_{\Delta\nu}/\Delta\nu$). For most host stars, $e_{\nu_{\max}}/\nu_{\max}$ and $e_{\Delta\nu}/\Delta\nu$ are less than 3 per cent. More precise asteroseismic parameters lead to a more accurate determination of stellar mass. According to the standard error propagation of the scaling relations, the relative uncertainty in mass mainly depends on three times the fractional uncertainty in $\nu_{\max}$ and four times that in $\Delta\nu$. Therefore, reducing the uncertainties in these parameters improves the precision of the mass estimate and, consequently, allows for a more reliable determination of the stellar age.

During the RGB phase, stars expand significantly and lose mass with cold stellar winds; after reaching their maximum radii at the tip of the RGB, they undergo a helium flash and enter the RC phase. While the radii of RGB stars can reach values of $\sim 50\,R_\odot$, RC stars typically have radii in the range of 8–21 $R_\odot$. However, planet engulfment primarily occurs near the RGB tip, where the stellar radius and tidal interactions are strongest. A planet may either directly enter the stellar envelope or spiral into the star due to strong tidal interactions. This implies that planets located within $\sim$ 50–60 $R_\odot$ of their host stars are likely to be engulfed, unless they have already undergone a prior interaction.

If a host is an RC star, then the period spacing ($\Delta\Pi_1$) is a significant constraint to model the interior of a star. Unfortunately, $\Delta\Pi_1$ is not available for any host taking place in the RC region in Fig. 3. In Fig. 3, $\nu_{\max}$ is plotted against $\Delta\nu$ for the host stars, whose asteroseismic parameters are compiled from the literature, and compared with RGB and RC stars from the APOKASC-2 sample. The majority of the host stars are located near the RC sequence. Among these, 12 stars have been classified as RC objects in the literature. However, the classification of other stars located within the RC region remains uncertain and requires further investigation.

The $\delta\nu_{02}$ values have been determined for 17 of the MS and SG stars, ranging from 4.3 to 9.0 μHz. $\nu_{\min0}$ and $\nu_{\min1}$ obtained from the $\Delta\nu$–ν plot are determined for 23 of the 133 host stars. For 6 stars, $\nu_{\min0}$ or $\nu_{\min1}$ is detected. $\nu_{\min0}$ and $\nu_{\min1}$ have values in the ranges 245–4221 μHz and 553–3849 μHz, respectively (see Table A1).

3 METHOD OF MODELLING

Instead of applying a single method to all stars during modelling, we used different methods based on the data in the literature and their uncertainties. These methods include MinZ, DZTR, DZTref, DZT, and DZTL. In addition, for 12 RC stars we applied two separate methods: DZLTeC and DZLTe3. The method names indicate the observational constraints used in the modelling:

(i) MinZ: 'Min' denotes the unique solution corresponding to the minimum χ^2, Z_s.
(ii) DZTR: $\Delta\nu$, Z_s, $T_{\rm eff}$, R.
(iii) DZT: $\Delta\nu$, Z_s, $T_{\rm eff}$.
(iv) DZTref: $\Delta\nu$, Z_s, $T_{\rm eff}$, the reference frequencies.
(v) DZTL: $\Delta\nu$, Z_s, $T_{\rm eff}$, L.

(vi) DZLTeC: $\Delta\nu$, Z_s, L, $T_{\rm eff}$, the mass-loss coefficient (η) is determined from model calibration (eC).

(vii) DZLTe3: $\Delta\nu$, Z_s, L, $T_{\rm eff}$, the mass-loss coefficient is fixed at $\eta = 0.3$ (e3).

Among these methods, MinZ represents the most reliable approach and provides a unique solution. This method requires high-quality asteroseismic data, and stars with detected individual oscillation mode frequencies are the most advantageous stars. In this case, we know that the model we obtained by using $\Delta\nu$, reference frequencies, and Z_s as constraints is the unique model (S. Örtel et al. 2025).

In the DZTR method, the $\nu_{\rm max}$ parameter is used when individually identified oscillation frequencies are available for stars. However, during the modelling of the stars, the seismic parameter that mainly affects the models and is used is $\Delta\nu$. The main reason for this is that the use of $\nu_{\rm max}$ in these scaling relations has three important disadvantages, particularly for MS and SG stars.

First, we cannot correct the relation of $\nu_{\rm max}$ to the fundamental parameters of the models. Secondly, the power spectra of hot F-type stars may exhibit more than one maximum, although this is not the case for all stars. In this study, there are two F-type stars with temperatures higher than 6000 K (KIC 9592705 and TIC 200723869). Third, the uncertainty in $\nu_{\rm max}$ is generally higher than the uncertainty in $\Delta\nu$: $e\nu_{\rm max}/\nu_{\rm max} = 6e_{\Delta\nu}/\Delta\nu$. For the TESS 2-min cadence light curves (J. Zhou et al. 2024), $e\nu_{\rm max}/\nu_{\rm max}$ and $e_{\Delta\nu}/\Delta\nu$ are high and close to each other. When we compare TESS and Kepler targets, we see that Kepler data have less uncertainty. For Kepler target stars, $e_{\Delta\nu}/\Delta\nu < 0.05$ and $e\nu_{\rm max}/\nu_{\rm max} < 0.02$. As a consequence, the stellar mass derived from the scaling relations becomes highly uncertain, because, as shown in equations (1) and (2), the stellar radius depends on $\nu_{\rm max}$ whereas the stellar mass depends on ${\nu_{\rm max}}^3$. Therefore, the uncertainty in mass is significantly larger than that in radius.

This study is based on high-quality spectroscopic and asteroseismic data. For a large fraction of the sample, the uncertainty in $\Delta\nu$ is below 2 per cent, while for most stars the uncertainty in $T_{\rm eff}$ is smaller than 100 K. For these stars, Y_0 and α can be determined through the calibration of stellar models under observational constraints. This approach applies to most host stars with available reference frequencies and is referred to as the DZTref method.

If the oscillation frequencies of the individual modes are not available in the literature, we compute $\Delta\nu$, Z_s, and $T_{\rm eff}$ as the observational constraints (Method DZT).

For some stars, the spectroscopic $T_{\rm eff}$ is quite uncertain. In such cases, we either use luminosity derived using GAIA data (Method DZTL) or radius computed from the scaling relations (Method DZTR).

For Methods DZT, DZTL, and DZTR, we assume that the chemical enrichment on the galactic disc proceeded as an increase in Y (ΔY) is twice the increase in Z (ΔZ): $\Delta Y = 2\Delta Z$. The heavy-element abundance can be determined from the stellar spectra. However, in order to determine the helium abundance of a star, either the solar initial helium abundance is adopted, or the helium abundance is calculated by assuming a relation between helium and metal enrichment. Although values of $\Delta Y/\Delta Z$ between 1 and 5 have been reported in the literature, a value of 2 is most commonly adopted (L. Casagrande et al. 2007; E. Tognelli et al. 2021). The values obtained with the ANKİ code (D. Ezer & A. G. W. Cameron 1965; M. Yıldız & N. Kızıloğlu 1997) and MESA are 1.95 and 1.58, respectively; therefore, we adopt $\Delta Y/\Delta Z = 2$ in this study.

It is well known that the star loses a significant amount of mass as it climbs the RGB branch, approximately 0.1–0.3 $M_\odot$ (T. Lebzelter & P. R. Wood 2011; A. Miglio et al. 2012). In cases where there is such a mass-loss, the planet is greatly affected for two reasons: First, since the central body loses mass, there is a significant change in the planet's orbit. Second, some of the mass lost by the star can be directly transferred to the planet, and in this case, the structure of the planet can change significantly. Such processes are complex, and depending on how mass accretion occurs, different outcomes can result. In this study, the mass-loss rate was investigated using Reimers' approach: mass-loss rate is proportional to $\eta LR/M$ (D. Reimers 1975).

For clarity, the methods used in this study can be summarized as follows:

(i) MinZ: When individual oscillation frequencies are available, the MinZ method provides a unique stellar model. This method was applied to a single star (KIC 8866102).

(ii) DZTR: In this approach, stellar radii were derived from scaling relations. A total of 13 stars are modelled using this method.

(iii) DZTref: This method was used for stars with high-quality asteroseismic and spectroscopic data, for which reference frequencies were available. 19 stars are analysed using this method.

(iv) DZT: For stars without reference frequencies in the literature and with consistent spectroscopic $T_{\rm eff}$ values, the DZT method was employed. The models of 46 stars are obtained using this method.

(v) DZTL: Since the spectroscopic $T_{\rm eff}$ values of some stars are highly uncertain, the luminosities were computed using *Gaia* data. This method was applied to 41 stars.

(vi) DZLTe3: 10 RC stars are analysed using this method. The mass-loss coefficient η is taken as 0.3. The mass of the hosts is computed from the scaling relation given below:

$$\frac{M_{\rm sca}}{{\rm M}_\odot} = \frac{(L/{\rm L}_\odot)^{3/2}}{(\langle\Delta\nu\rangle\,/\,\langle\Delta\nu_\odot\rangle)^2}\left(\frac{{\rm T}_{\rm eff\odot}}{T_{\rm eff}}\right)^6. \qquad (3)$$

(vii) DZLTeC: This method is similar to DZLTe3 and is also applied to 2 RC stars. The mass-loss coefficient η is found from calibration of models.

After summarizing the methods, the modelling procedure for the host stars can be described as follows: First, we compute the fundamental stellar parameters using the modified scaling relations. Then, we compare these results with the model results with the closest values of Z and M in the HRD. If there is a good agreement, then this model is the best model for the host star. If not, we test other M and Z combinations.

The chemical composition of a star is among the most influential initial essential properties. Metallicity, in particular, significantly affects the structure of the nuclear core and the outer regions. Therefore, it is one of the most important ingredients of the interior models, after the stellar mass. In all the methods for asteroseismic modelling, we first use Z_0 calculated from the observed metallicity of the hosts. According to the difference between Z_0 and Z_s, we estimate a new Z_0. The initial model value of Z_0 is taken to be approximately 10 per cent higher than Z_s, since some of these stars are in the middle and late stages of their MS evolution. An iterative procedure is then applied until consistency between Z_0 and Z_s is achieved. For the evolved RGBs, Z_0 is close to Z_s.

3.1 Properties of MESA evolution code

Nonrotating interior models of the planet hosts are constructed using MESA code version r23.05.1. Element diffusion is applied using the method proposed by C. Paquette et al. (1986) for the stars with $M < 1.4\ M_\odot$. For the higher masses, the models are without diffusion. The standard mixing length theory proposed by E. Böhm-Vitense et al. (1958) is used for the convection. The opacity is computed using OPAL tables (C. A. Iglesias & F. J. Rogers 1993, 1996) at high temperature and the tables of J. W. Ferguson et al. (2005) at low temperature. Depending on the current state of evolution of the stars, the internal structure models cover pre-MS, MS, SG, and RGB phases.

In MESA, different equations of state (EOS) are blended depending on the temperature-density regime. For the stars studied here (MS, SG, RGB, and RC phases), most of the stellar models lie within the regime covered by FreeEOS.[1]

The adiabatic oscillation frequencies of the fitted model are computed using the ADIPLS package (J. Christensen-Dalsgaard 2008). To account for the surface effect, the correction proposed by H. Kjeldsen, T. R. Bedding & J. Christensen-Dalsgaard (2008) is applied.

4 RESULTS AND DISCUSSIONS

4.1 Model properties across the observed properties

In Fig. 4(a), the observed large frequency separation ($\Delta\nu_{\rm obs}$) of the host stars is compared with the model values ($\Delta\nu_{\rm mod}$). $\Delta\nu_{\rm mod}$ shows an excellent match with $\Delta\nu_{\rm obs}$, confirming the reliability of the modelling.

Fig. 4(b) shows the comparison between observed ($T_{\rm obs}$) and modelled effective temperatures ($T_{\rm mod}$). Overall, $T_{\rm obs}$ and $T_{\rm mod}$ are in perfect agreement, although some scatter is visible. This scatter is likely due to the relatively significant uncertainties in the observed stellar temperatures.

4.2 Planet hosts in the RC evolutionary phase

A star that has passed the RGB tip and reached the RC region has experienced significant mass-loss. Even if we can accurately determine the present-day M and R of an RC star from modelling or scaling relationships, determining the amount of mass-loss is crucial because age largely depends on the initial mass. The coefficient η is taken as 0.3 for the 10 hosts. For the two hosts, namely TIC 257005016 and TIC 284181945, we obtain the best models with η=0.42 and 0.58, respectively. The basic properties of the models are listed in Table 1.

In Fig. 5, details of the RC model of TIC 257005016 are shown. In the upper panel, $\Delta\nu$ is plotted with respect to $T_{\rm eff}$ from the zero-age core helium burning (ZACHeB) to the terminal-age core helium burning (TACHeB). The host initially rises slightly and then descends considerably. Observations only align with this when it is at the peak of its evolutionary trace. The middle panel shows the host's mass versus Z. Although the Z is very close to the initial value of Z_0 in the outer parts, it rises to 0.06 in the core as ^{4}He is converted to ^{12}C. Interestingly, the helium flash leaves a relatively irregular Z distribution in the core.

[1] https://freeeos.sourceforge.net/

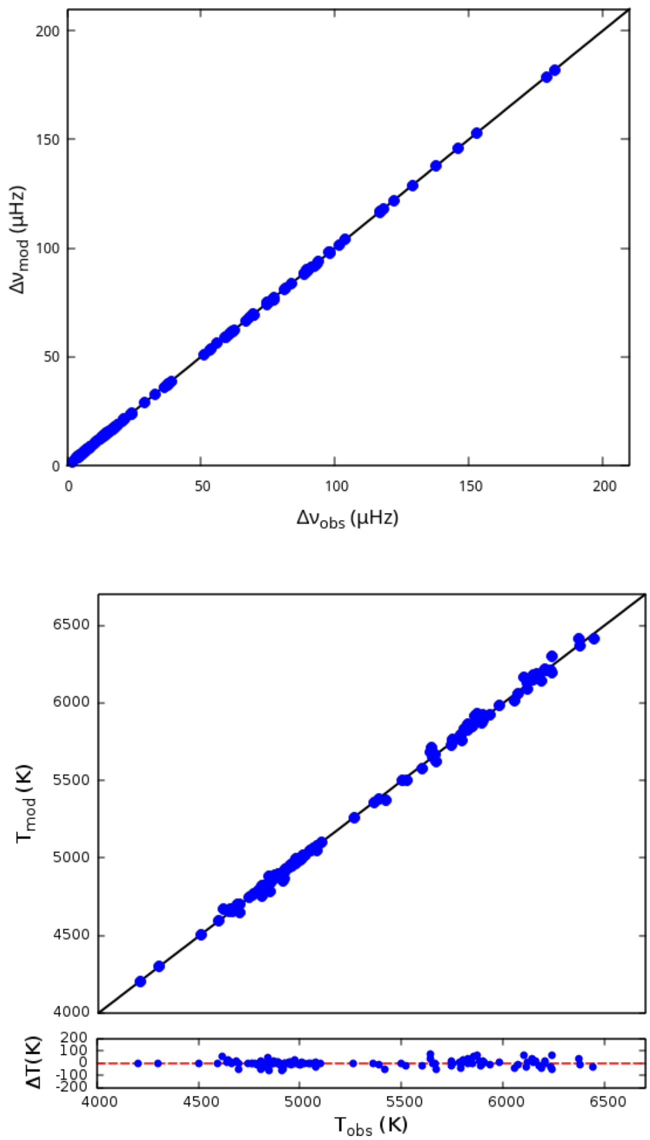

Figure 4. (a) $\Delta\nu_{\rm mod}$ is plotted with respect to $\Delta\nu_{\rm obs}$. For most of the hosts, the difference between $\Delta\nu_{\rm mod}$ and $\Delta\nu_{\rm obs}$ is less than 1 per cent for most of the hosts. (b) $T_{\rm mod}$ is plotted with respect to $T_{\rm obs}$. The difference between $T_{\rm mod}$ and $T_{\rm obs}$ is less than 50 K for most of the hosts.

4.3 Are diving (dalgıç) planets real?

The bottom panel of Fig. 5 shows the time variation of TIC 257005016's radius near the RGB tip ($R_{\rm tip}$). This star's radius grows to 0.7 au, whereas TIC 257005016b's a is 0.49 au. The host's R is greater than a for approximately 1 Myr, starting from 1.79 Gyr. How can this happen? Two more stars have $R_{\rm tip}$ values exceeding the a of their planets. These stars are TIC 129649472 and TIC 160224839. How could the planet have survived? The survival of planets around evolved stars has been widely discussed in the literature (E. Villaver & M. Livio 2007; M. Kunitomo et al. 2011; C. E. O'Connor et al. 2023). In particular, M. Hon et al. (2023) discussed the survival of 8 UMi b (TIC 257005016), and proposed explanations for its survival. Considering both previous studies and our results, we discuss the following possible scenarios: (i) The density of the outer layers around the RGB tip is very low; the planet may have dived and resurfaced. (ii) These planets may be second-generation planets formed in the disc created by the

Table 1. The interior models of 12 RC stars are constructed with mass-loss. The mass is mostly lost around the RGB tip. Initial and final masses are listed in the second and third columns, respectively. The Reimer coefficient and the amount of lost mass are given in the third and fourth columns, respectively.

Host	M_0 $\mathrm{M_\odot}$	M $\mathrm{M_\odot}$	η	ΔM $\mathrm{M_\odot}$
TIC 17554529	2.395	2.387	0.300	−0.008
TIC 28763463	1.754	1.684	0.300	−0.071
TIC 49430557	1.794	1.725	0.300	−0.069
TIC 129649472	1.174	1.036	0.300	−0.138
TIC 160224839	0.974	0.814	0.300	−0.160
TIC 232074535	1.952	1.901	0.300	−0.050
TIC 246937460	1.196	1.074	0.300	−0.122
TIC 247119634	1.822	1.750	0.300	−0.072
TIC 257005016	1.666	1.556	0.420	−0.109
TIC 284181945	2.227	2.185	0.580	−0.042
TIC 354489950	2.390	2.385	0.300	−0.005
TIC 441797545	1.410	1.314	0.300	−0.096

mass lost by the host. (iii) If the planet gained some of the mass lost by the host, it may have been dragged towards the host as M_{p} increases and its a decreases. (iv) The host's initial mass may be much greater, in which case $R_{\mathrm{tip}} > a$ would not be true since R_{tip} is lower. Investigating planetary hosts in the RC phase is of particular importance as it is also crucial for understanding the ultimate end of Earth.

4.4 Thick disc members

Three of the 127 hosts, namely KIC 6278762, TIC 136916387, and TIC 160224839, have [α/Fe] values of 0.26, 0.15, and 0.19, respectively. The basic properties of the models are listed in Table 1. (T. L. Campante et al. 2015; D. K. Feuillet et al. 2016; A. Weeks et al. 2025). Since the [α/Fe] of these three stars is greater than 0.1 dex (A. Miglio et al. 2021), these stars are thick disc members and among the oldest hosts (see Fig. 7). For these stars, the observed [Fe/H] and [α/Fe] values were used to calculate the metallicity [M/H] using the relation of M. Salaris, A. Chieffi & O. Straniero (1993). The corresponding Z_{s} values were then calculated from [M/H]. Since these stars are evolved, we adopted $Z_0 \approx Z_{\mathrm{s}}$ and used this value as the metallicity input in the models. These models were then used to determine R_{tip}.

4.5 Asteroseismic HR diagram

The age of a star is a key parameter for understanding its internal structure and the evolution of stellar and planetary systems. Asteroseismology enables the determination of stellar ages with significantly higher precision than other methods. An asteroseismic HRD is an effective tool for this purpose (J. Christensen-Dalsgaard 1993).

In Fig. 6, the $\Delta\nu$ is plotted against the small frequency separation to construct an asteroseismic HRD for the host star models. In this diagram, solid lines indicate stellar mass (1.4 $\mathrm{M_\odot}$ on the left and 0.8 $\mathrm{M_\odot}$ on the right), while dashed lines indicate the MS phases (ZAMS at the top and TAMS at the bottom). The least evolved star in the MS phase is KIC 4141376, with a $\delta\nu_{02}$ of 11.9 μHz. Two more systems have not yet reached the halfway point of their MS lives; these are KIC 6278762 and KIC 8478994. These stars have $\delta\nu_{02}$ around 10.5 μHz. Since the masses of both stars are less than 0.8 $\mathrm{M_\odot}$, they are located to the right of the 0.8 $\mathrm{M_\odot}$

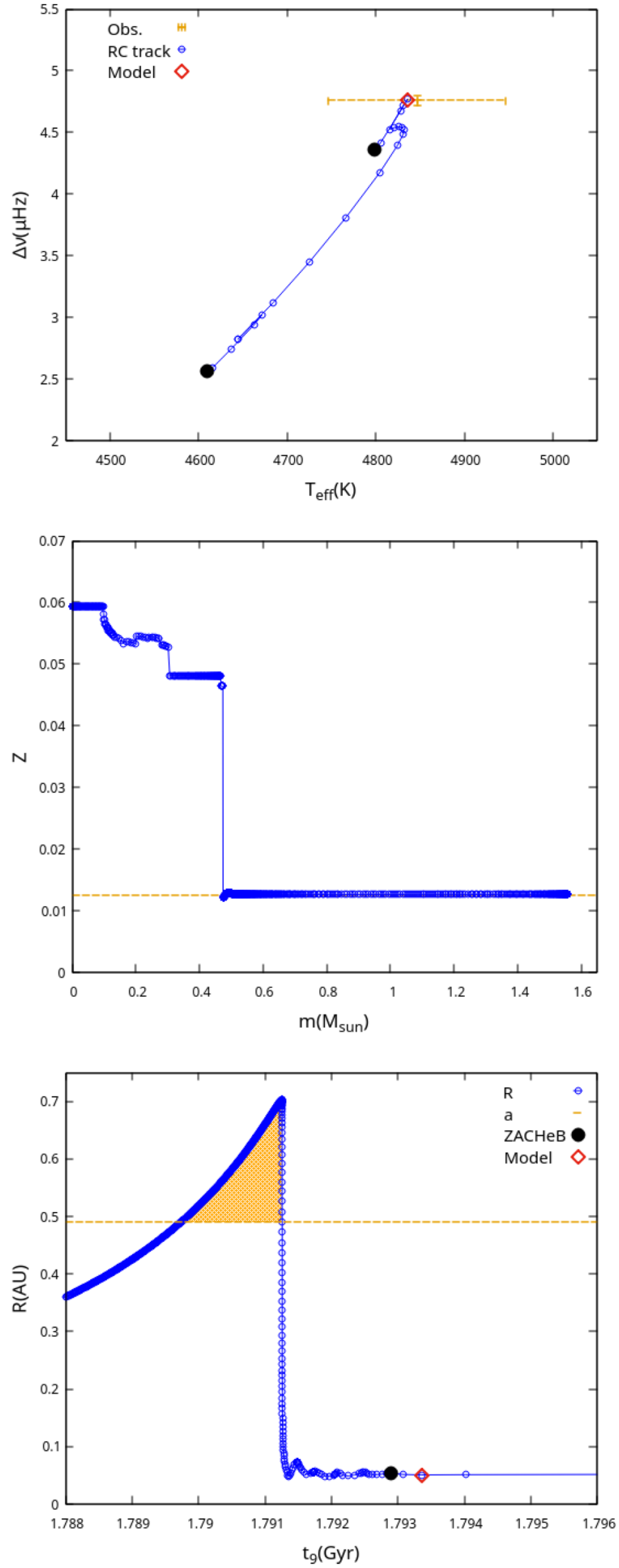

Figure 5. (a) Evolutionary track of TIC 257005016 is plotted in the $\Delta\nu$-T_{eff} graph. (b) Z throughout the interior model is plotted with respect to m. In the core region, Z is significantly greater than Z_0, where the triple alpha process produces ^{12}C. (c) TIC 257005016's age versus radius. The dashed lines indicate the distance of the planet from its host star. The planet TIC 257005016b may be a diving planet.

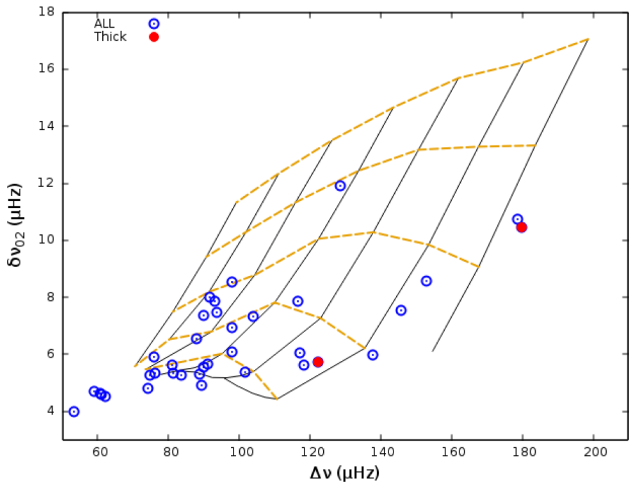

Figure 6. Asteroseismic HRD for models of the hosts. The grids are prepared for $M = 0.8 - 1.4\ \mathrm{M}_\odot$ with steps of $0.1\ \mathrm{M}_\odot$ and $Z_0 = 0.02$ (nearly vertical solid lines). The dashed lines show the evolutionary phases from ZAMS (at the top) to TAMS (at the bottom). The solid circles represent the thick stars KIC 6278762 and TIC 136916387.

line. The stars form two clear groups: one is concentrated near the TAMS, while the others appear to have completed about three-quarters of their MS lifetime.

4.6 Metallicity–age relationship

The Z_0–t_9 relationship obtained from host internal-structure models is shown in Fig. 7. This figure shows two interesting features. One of these is about galactic chemical evolution: For stars formed from gas clouds with the fastest increasing metallicity, there is a linear relationship between Z_0 and $t_0 = t_{\mathrm{MW}} - t_9$. t_{MW} is taken as 13.4 Gyr (L. Pasquini et al. 2004).

Old stars formed in the early epochs of the Milky Way generally exhibit lower metallicities, while younger stars exhibit higher metallicities. This trend is consistent with expectations from galactic chemical evolution. Another critical point is that no planetary systems are found below a certain metallicity threshold. In our samples, we observe that host stars with $Z_0 < 0.007$ do not harbour planetary systems. This may be the main link between stellar metallicity and the occurrence of planetary systems. Hence, this aspect plays a crucial role in studying stellar-planetary evolution and in improving our understanding of planet formation processes.

Some host stars exhibit very low measured [M/H] ([Fe/H]) ratios, corresponding to low Z_s values (W. D. Cochran et al. 2007; F. Dai et al. 2023). This arises from the difference between Z_0 and Z_s. In particular, stars evolving along the MS exhibit low Z_s. After the MS, however, as the convective envelope deepens and previously buried heavy elements are transported back to the surface, Z_s approaches Z_0 (see Appendix B for further details).

4.7 The initial metallicity versus surface metallicity

The initial metallicity plays a key role in determining the structure of stars. Because more energy is expended on ionization when the number of heavy elements is high, less of the energy gained from the collapse during star formation is spent on heating the deep interior. In this case, the temperature increases less, leading to slower nuclear reactions and lower luminosity. From this perspective, the initial Z has a significant impact on the

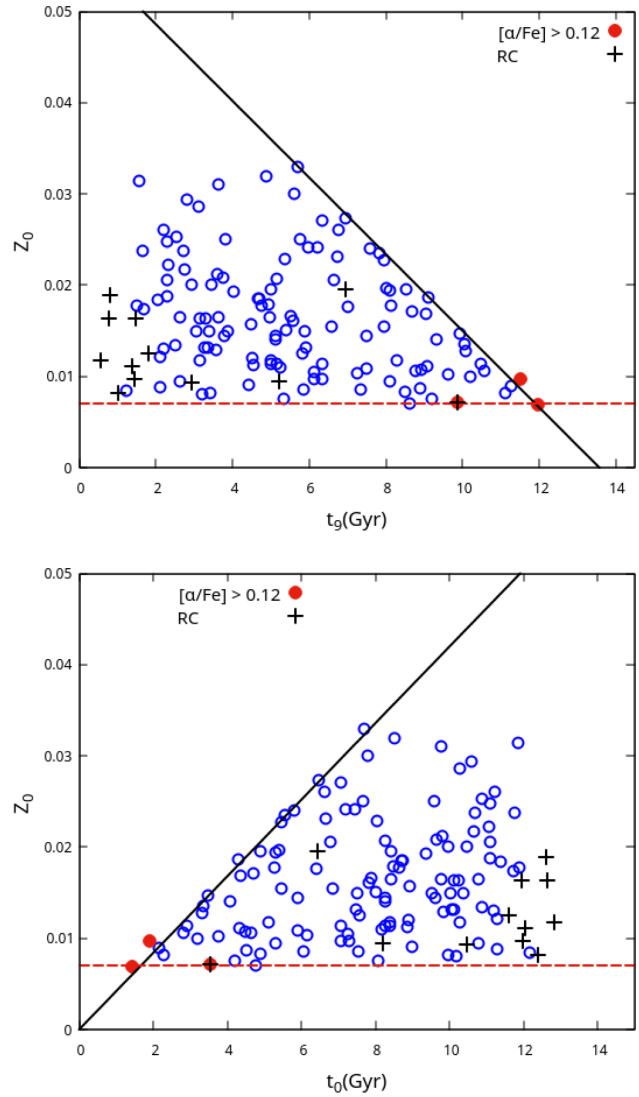

Figure 7. (a) Z_0 as a function of stellar age (t_9). The solid line is the border for the stars with the highest metallicities of their ages, expressed as $Z = -0.00395 t_9 + 0.053$. The dashed line indicates $Z_0 = 0.007$, above which all host stars in our sample are located. While the filled circle shows the thick disc members ($[\alpha/\mathrm{M}] > 0.12$), the cross is for the RC stars. (b) Z_0 as a function of t_0, defined as $t_0 = t_{\mathrm{MW}} - t_9$, where $t_{\mathrm{MW}} = 13.4$ Gyr.

structure of stars (especially on their luminosity). Z, determined from spectral observations, is actually the surface heavy element abundance Z_s. Structure and evolution, in turn, depend primarily on Z_0. The crucial question here is whether we can calculate Z_0 from Z_s.

Using the data of host interior models, the fractional difference $\Delta Z/Z_s$ ($(Z_0 - Z_s)/Z_s$) is plotted against R in Fig. 8(a). The difference is particularly significant for the range $R < 3\ \mathrm{R}_\odot$. For larger radii, the deepening convective envelope eliminates the chemical separation caused by microscopic diffusion. For $R < 3\ \mathrm{R}_\odot$, R roughly represents the evolutionary state. The diffusion effect depends on the depth of the convective envelope. The depth of the convective envelope depends on M and Z. Then we can consider $\delta Z/Z_s$ as a function of M, Z_s, and R: $f(M, Z_s, R)$. We assume a function as:

$$\frac{\delta Z}{Z_s} = f(M, Z_s, R) = b\frac{M}{M_\odot} + cZ_s + d\frac{R}{R_\odot}. \quad (4)$$

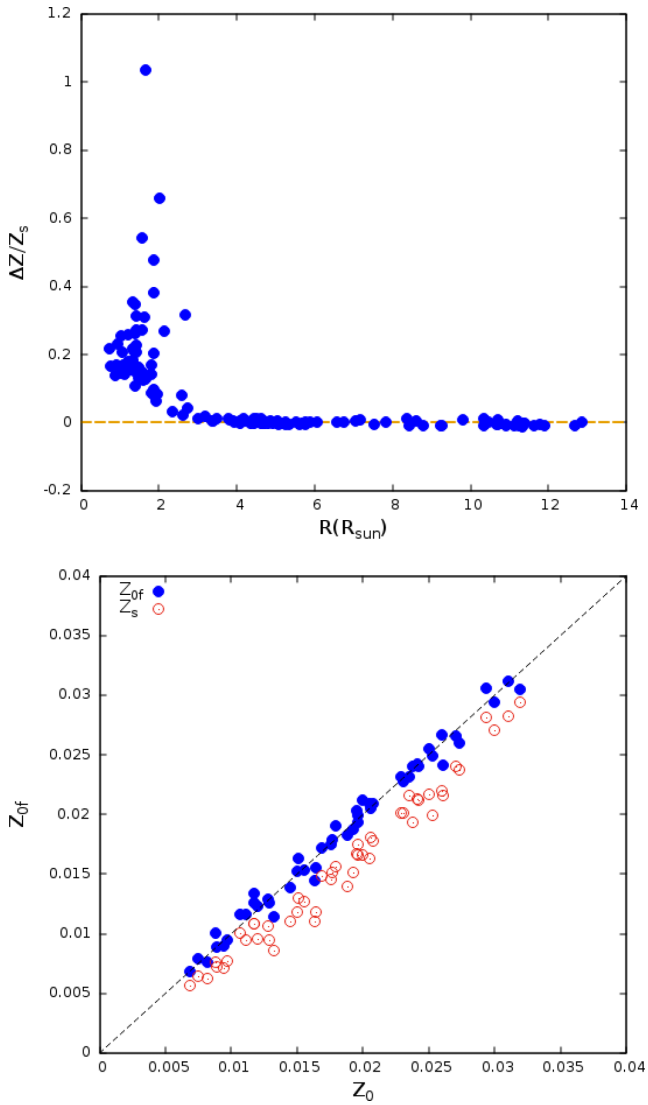

Figure 8. (a) The fractional difference between Z_0 and Z_s is plotted with respect to radius for the interior models of the hosts. The greatest difference is for KIC 11401755. While its Z_0 is 0.011, its Z_s is about half of Z_0. The second greatest difference occurs for KIC 10666592. The difference is due to microscopic diffusion and is significant for the stars with $R < 3\mathrm{R}_\odot$. Assuming the difference is a function of M, Z_s, and R, we obtain a fitting formula for these stars, except KIC 10666592 and KIC 11401755. (b) Z_{0f} (filled circles), computed from the fitting formula, is plotted against the original Z_0. Also plotted is the Z_s (circles).

From this function, we obtain the fitting formula using the data of 50 hosts for which $dZ > 0.0005$. Then, we can compute Z_0 in terms of M, Z_s, and R:

$$Z_{0f} = Z_s(1 + f) \tag{5}$$

In Fig. 8(b), Z_{0f} is plotted with respect to Z_0. The metallicities calculated from the model and the Z_0 relationship are in excellent agreement.

In our host sample, there are a few stars in the vicinity of the ZAMS. Therefore, equation (4) is only valid for evolved MS and SG stars. For the young stars, $\delta Z/Z_s$ is a double-valued function of R.

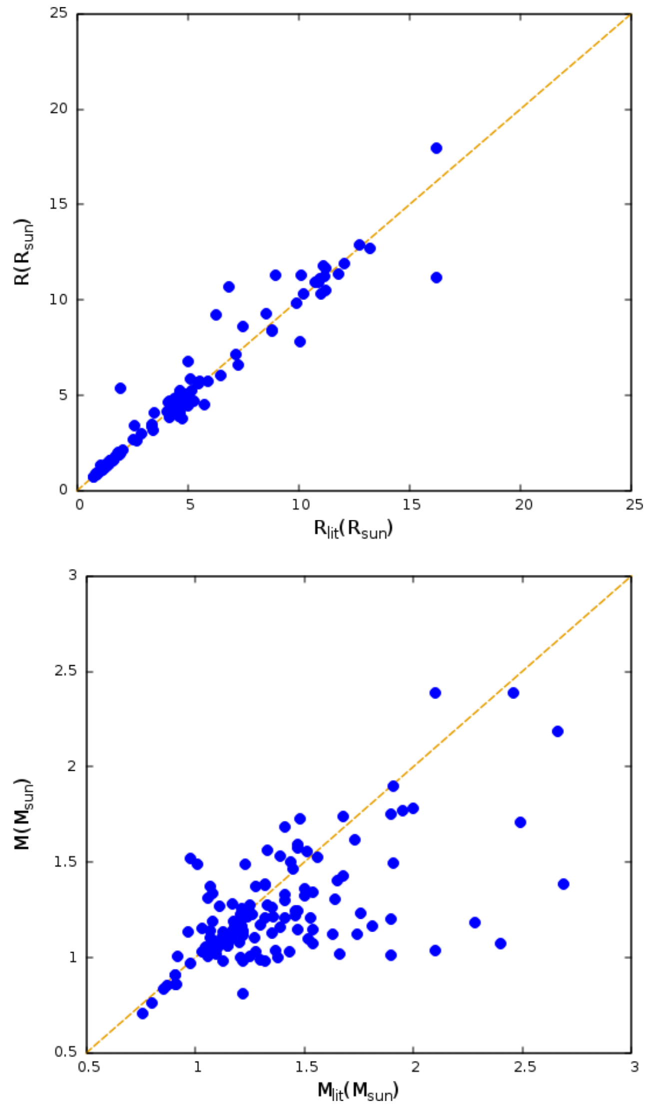

Figure 9. (a) R is plotted with respect to $R_{\rm lit}$ for the 127 planet hosts. The radii are in good agreement with the literature. (b) M is plotted with respect to $M_{\rm lit}$. In contrast, the masses show a larger scatter.

4.8 Comparison of stellar radius and mass with the literature

In Figs 9(a) and (b), the radii and masses of the models are compared with the radii ($R_{\rm lit}$) and masses ($M_{\rm lit}$) from the literature, respectively. The scatter in the radii is significantly smaller than that in the masses. This is expected, since the radii can be more directly constrained from observational quantities such as luminosity (e.g. from *Gaia*) and effective temperature. In contrast, masses are usually derived from $\log g$ and R. Therefore, uncertainties in different observational parameters affect the mass estimates. In particular, the poor determination of $\log g$ leads to a larger scatter in the masses.

The use of scaling relations without corrections, especially for RGB and SG stars, also contributes to the scatter in the derived masses and radii. Previous studies have shown that the classical asteroseismic scaling relations for red giants do not exhibit a direct dependence on metallicity. However, the corrected asteroseismic scaling relations show a dependence on metallicity through both the $\Delta\nu \propto \sqrt{\bar{\rho}}$ relation (Fig. 5; M. Yıldız 2023) and the $\nu_{\rm max} \propto g/\sqrt{T_{\rm eff}}$ relation (equation 11; M. Yıldız 2023). Applying these corrections significantly improves the agreement between asteroseismic and dynamical parameters. In particular, M. Yıldız, S. Örtel & T. Çakır Alsaç (2026) showed that the corrected radius scaling relation ($R_{\rm sca}$) reproduces the dynamically measured radii of red giants in eclipsing binaries with excellent accuracy. The corrected mass scaling relation ($M_{\rm sca}$) likewise improves the agreement with dynamical masses, although a somewhat larger scatter remains. These studies cover a wide range of metallicities, including those of the stars in our sample.

In this comparison, we ensured that the $M_{\rm lit}$ and $R_{\rm lit}$ were taken from the same source that provides the planetary parameters. It should be noted that the masses and radii adopted from the literature were not derived using a single homogeneous method. Most of the literature values were obtained from asteroseismic analyses (e.g. D. Huber et al. 2013a), whereas the remaining values were primarily derived through isochrone fitting or grid-based modelling using spectroscopic and photometric constraints (e.g. J. M. Brewer et al. 2016; R. A. Wittenmyer et al. 2017a; H.-Y. Teng et al. 2023). Since these methods rely on different assumptions and have different systematic uncertainties, part of the scatter observed in the mass and radius comparisons shown in Fig. 9 is expected.

4.9 Revised radius and mass of the planets

Due to two spheres passing in front of each other, the light curve of a planetary system changes. The transit depth, ΔF, with F defined as the total observed flux, is given as (S. Seager & G. Mallén-Ornelas 2003)

$$\Delta F = \left(\frac{R_{\rm p}}{R}\right)^2. \tag{6}$$

Since the radius ratio will be constant for a given value of ΔF, we can also calculate the revised $R_{\rm p}$ ($R'_{\rm p}$) from the newly calculated R of the host. $R'_{\rm p}$ is also listed in Table A2. The fractional difference between $R'_{\rm p}$ and $R_{\rm p}$ ($(R'_{\rm p} - R_{\rm p})/R_{\rm p}$) is plotted with respect to R in the upper panel of Fig. 10. The difference is less than 10 per cent.

The revised planetary mass is computed from the ratio of the new stellar mass to the old one. In the lower panel of Fig. 10, the fractional difference between $M'_{\rm p}$ and $M_{\rm p}$ ($(M'_{\rm p} - M_{\rm p})/M_{\rm p}$) is plotted against R. For most planets, the difference is quite large, reaching up to 50 per cent. This difference is due to the difference between the new stellar mass and the old mass. For TIC 200093173b, the difference is about 55 per cent. The mass of the host is given as 0.98 ± 0.125 M$_\odot$ in F. Feng et al. (2022) and is found to be 1.517 M$_\odot$ in the present study. It is worth noting that $M_{\rm p}$ here is mainly $M_{\rm p} \sin i$. See Fig. C1 in Appendix C for the differences between revised and literature values of radius and mass of the planets and the hosts.

4.10 Expression for $M'_{\rm p}$ as a function of a and M

In Fig. 10, $M'_{\rm p}$ is plotted with respect to M and a in logarithmic scales. The grids show the fitted function $f(x, y)$:

$$\log\left(\frac{M'_{\rm p}}{\rm M_J}\right) = (1.10 \pm 0.35)\log\left(\frac{M}{\rm M_\odot}\right) + (1.07 \pm 0.07)\log\left(\frac{a}{AU}\right). \tag{7}$$

According to this relationship, the planetary mass increases with increasing M and a. This result is interesting because it may

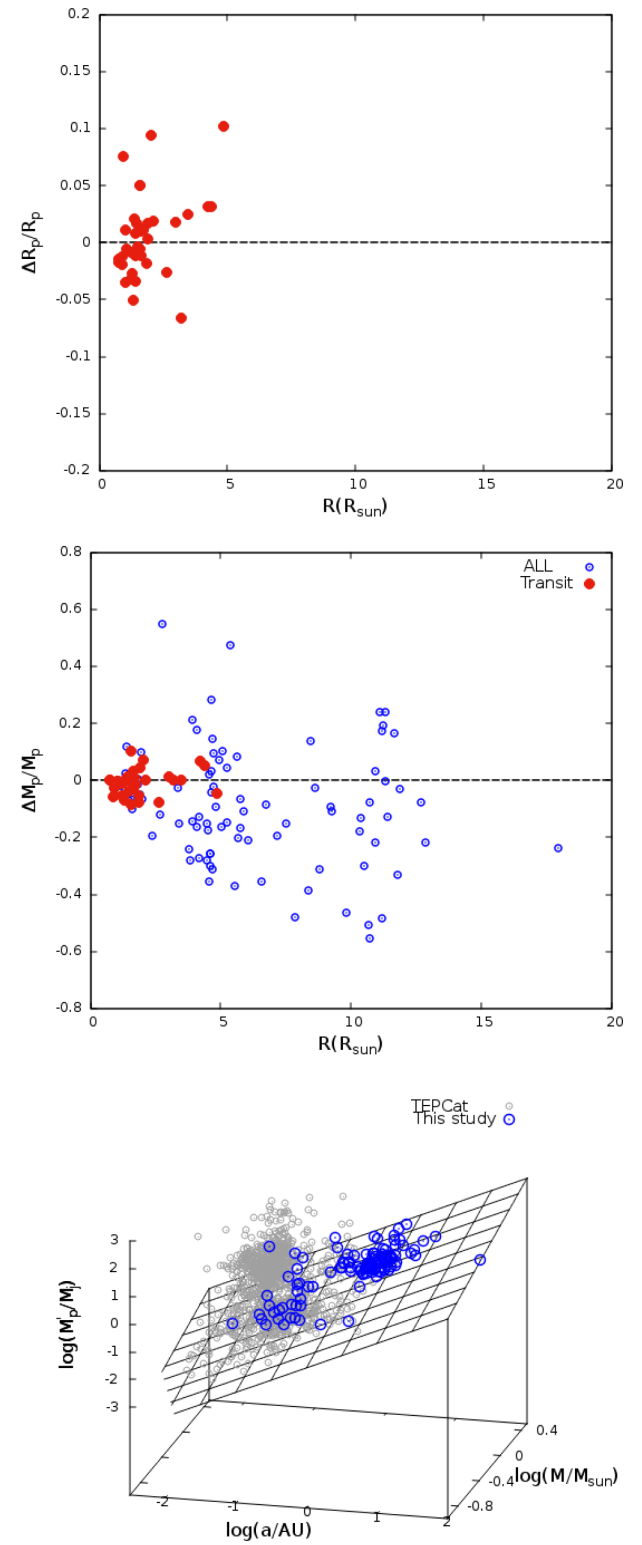

Figure 10. (a) $(R'_{\rm p} - R_{\rm p})/R_{\rm p}$ and (b) $(M'_{\rm p} - M_{\rm p})/M_{\rm p}$ are plotted with respect to R of the hosts. Radii of the transit planets are determined from the observations in units of their host radii (filled circles). The difference for $R_{\rm p}$ is less than 10 per cent for 37 transit planets. For these planets, the difference for M_p is similar to that of R_p. However, for all of the planets (circle), the difference is less than 50 per cent. (c) In the lower panel, $M'_{\rm p}$ is plotted with respect to a and M in logarithmic scales.

indicate the density that existed under the conditions of the disc (presumably in the inner parts of the disc) that produced the planet with mass $M'_{\rm p}$. Other systems in the TEPCat catalogue (J. Southworth 2011) are also plotted for comparison. We observe that there are many hot Jupiters in TEPCat with $M'_{\rm p} > 0.3$ M$_{\rm J}$ and $a < 0.1$ au. However, such hot Jupiters are relatively rare among the b planets of our 127 hosts. Hot Jupiters form a distinct group, and therefore equation (7) is not valid for them.

The fact that our sample does not contain many hot Jupiters around stars exhibiting solar-like oscillations is noteworthy. Although it is widely accepted that hot Jupiters reach their close-in orbits through migration processes (D. N. C. Lin, P. Bodenheimer & D. C. Richardson 1996; R. I. Dawson & J. A. Johnson 2018), tidal interactions during stellar evolution may lead to the engulfment of close-in giant planets by their host stars (E. Villaver & M. Livio 2009). It has been suggested that this effect is more pronounced for higher-mass evolved stars ($M_\star > 1.5\,M_\odot$; M. Kunitomo et al. 2011). However, the mass of most stars in our sample is below this threshold. Therefore, planetary engulfment alone is unlikely to explain the paucity of hot Jupiters in our sample. Furthermore, Fig. 10 represents only a subset of our sample, as planetary masses are not available for many systems. If the masses of these planets are determined in future studies, some could be classified as hot Jupiters, potentially increasing the observed hot Jupiter population. Hence, whether selection effects contribute to the paucity of observed hot Jupiters should be evaluated in more detail.

In contrast, while there are many planets with $M'_{\rm p} > 1$ M$_{\rm J}$ and $a > 1$ au in this study, planets in this region are rarely seen in the TEPCat catalogue. The radii of the hosts of these planets exceed 3.5 R$_\odot$.

4.11 How $R_{\rm p}$ depends on $M_{\rm p}$ and orbital parameters?

It is well known that there are three distinct *M–R* relationships for planetary mass ranges: rocky, Neptune-like, and Jovian. For the latter two in particular, the *M–R* relationship exhibits significant scattering. The host's irradiation flux plays a significant role in this scattering. A much more precise relationship emerges when the irradiated energy per gram per second (l_-) is used instead of the flux (M. Yıldız et al. 2014). In addition to these parameters, $R'_{\rm p}$ shows a secondary dependence on the orbital period *P*. The fitting formula for $R'_{\rm p}$ ($R'_{\rm pfit}$) is obtained as

$$\log\left(\frac{R'_{\rm pfit}}{\rm R_J}\right) = (-1.39 \pm 0.20) + (0.300 \pm 0.039)\log\left(\frac{l_-}{l_0}\right) +$$
$$(0.411 \pm 0.027)\log\left(\frac{M'_{\rm p}}{\rm M_J}\right) + (0.420 \pm 0.067)\log\left(\frac{P}{\rm day}\right), \quad (8)$$

where l_0 is the energy received per unit mass and time by a planet with 1 M$_{\rm J}$ and 1 R$_{\rm J}$ at 1 au in our Solar System ($l_0 = 1.106 \times 10^{-4}$ erg g^{-1} s^{-1}).

In Fig. 11, $R'_{\rm pfit}$ is plotted with respect to $R'_{\rm p}$. The average difference between $R'_{\rm pfit}$ and $R'_{\rm p}$ is approximately 14 per cent. The biggest difference is for KIC 8494142b, about 43 per cent. (The host star TIC 612908 was excluded from the plots in Fig. 11, because this planet has a very large radius despite having low incident flux.)

Another notable feature in Fig. 11(a) is that the agreement improves when $R'_{\rm p}$ is expressed as a function of the orbital parameters (*a* and *P*). In this case, the data points show less scatter, with better agreement between $R'_{\rm pfit}$ and R'p.

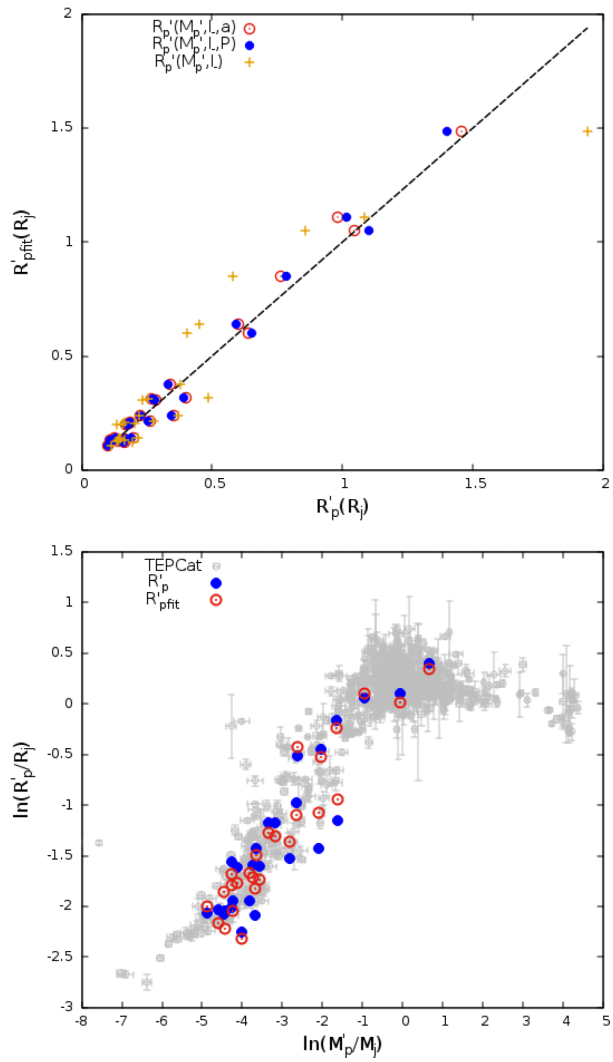

Figure 11. (a) $R'_{\rm pfit}$ (filled circle) given in equation (8) is plotted with respect to $R'_{\rm p}$. We obtain another fit for $R'_{\rm p}$ by substituting *a* (circle) for *P* in equation (8). The two fits give similar results. To see the direct effect of the orbital parameters, we obtain an expression as a function of $M'_{\rm p}$ and l_- (+). The $R'_{\rm pfit}$ obtained from this expression is not in good agreement with $R'_{\rm p}$. (b) $\ln(R'_{\rm p})$ (filled circle) and $\ln(R'_{\rm pfit})$ (circle) are plotted with respect to $\ln(M'_{\rm p})$. For comparison, the planets in TEPCat are also shown (grey errorbars).

4.12 Notes on individual hosts

4.12.1 16 Cyg B (KIC 12069449)

The asteroseismic data of 16 Cyg B is obtained from Kepler light curves (T. S. Metcalfe et al. 2012). Its individual oscillation frequencies are derived from this data. Its $\delta\nu_{02}$ is 6.6 μHz and is an essential constraint on age indicators. While its $\nu_{\rm min0}$ is well defined, $\nu_{\rm min1}$ is around the first interval of the data (2044 μHz). Detailed interior models of 16 Cyg A and B are constructed by T. S. Metcalfe et al. (2012) using different codes. *M*, *R*, and age are found to be 1.07±0.02 M$_\odot$, 1.127±0.007 R$_\odot$, and 6.7±0.4 Gyr, respectively. These models are in good agreement with the asteroseismic and non-asteroseismic data of these stars. Perhaps the low value of Y_0 is controversial. While the adopted Z_0 of 16 Cyg B (0.024) is greater than the solar value, the Y_0 of all models

Table 2. Basic properties of four interior models for TIC 95473936. Z_0 and α of the models are 0.0117 and 1.8311, respectively.

M $\mathrm{M}_\odot$	R $\mathrm{R}_\odot$	Y_0	$T_{\rm eff}$ K	L $\mathrm{L}_\odot$	$\Delta\nu$ μHz	$\nu_{\max}$ μHz	t_9 Gyr
1.001	1.869	0.28556	5493	2.865	53.80	912	8.44
1.012	1.879	0.28056	5494	2.897	53.67	910	8.39
1.034	1.897	0.27056	5498	2.963	53.61	908	8.29
1.045	1.907	0.26556	5499	2.995	53.48	906	8.25
1.059	1.919	0.25907	5499	3.037	53.33	904	8.19
Obs.	–	–	5501	3.038	53.67	939	–

(averaging 0.25) is much smaller than the solar value. This Y_0 is close to the primordial helium abundance (0.2471; Planck Collaboration VI 2020).

The fact that the models have high Z_0 (0.020–0.025) and quite small Y_0 (0.24–0.26) leads us to doubt their validity. Taking a high Z_0 increases the M of the calibrated model. In this study, we set $Z_0 = 0.0177$. The model we obtained with $M = 0.97$ $\mathrm{M}_\odot$ and $R = 1.10$ $\mathrm{R}_\odot$ is in good agreement with observational constraints. For this well-fitting model, Y_0 is 0.2825. The $\Delta\nu$, ν_0, and $\delta\nu_{02}$ of this model are in excellent agreement with the observational values. The difference between the observational ν_0 and the model ν_0 (13 μHz) is much smaller than $\Delta\nu$ (116.9 μHz), while the model and observational $\delta\nu_{02}$ are close.

4.12.2 KIC 6278762

KIC 6278762, with an estimated age of 11.98 Gyr, is the oldest star in our sample and stands out as one of the oldest known planet-host systems. The observational asteroseismic parameters are high-quality, and the spectroscopic [M/H] and $T_{\rm eff}$ values reported in the literature show strong consistency. For this star, the observed $T_{\rm eff}$ is 5046 ± 74, K, in excellent agreement with our model value (5046 K), further supporting the reliability of the adopted model.

4.12.3 70 Vir (TIC 95473936)

Numerous spectral analyses have been conducted for this star. [M/H], log(g), and $T_{\rm eff}$ were determined in the analysis from 52 references in the literature. According to these data, there are linear relationships between $T_{\rm eff}$ and log(g), and between [M/H] and log(g). log(g) = 3.90, determined by asteroseismic data. The most suitable data for this value are [M/H] = −0.09 and $T_{\rm eff}$ = 5501 K (D. Mahdi et al. 2016).

We obtained five different solutions that are close to each other. The properties of these models are listed in Table 2. Although the asteroseismic data are similar, only the input parameters M and Y_0 differ. Model masses range from 1.001 to 1.059 $\mathrm{M}_\odot$, and Y_0 ranges from 0.25907 to 0.28556. Y_0 decreases as the model mass increases. These models have two notable features. First, the model $\nu_{\max}$ values are smaller than the observational $\nu_{\max}$ values. Second, the age remains almost constant across different values of M and Y_0. This demonstrates that such an analysis is successful in determining the age but limited in determining the chemical composition of such stars.

The star is close to $L_{\max}$ in the SG. It appears 200 K colder than that point. The TIC catalogue gives $L = 3.038 \pm 0.081$ $\mathrm{L}_\odot$, and the model with the best fit for this luminosity has a mass of 1.059 $\mathrm{M}_\odot$. Table 2 demonstrates the significant strengths of asteroseismic modelling. While we can determine the age quite precisely, a good estimate of the chemical composition also requires a precise measurement of the observed luminosity. For this example star, $Z_0 = 0.0117$ and $Y_0 = 0.25907$.

4.12.4 KIC 4143755

This host is one of the lowest-mass stars in our catalogue. Literature data for this system are generally consistent. However, there is a significant difference between the model and spectral $T_{\rm eff}$ values. G. R. Davies et al. (2016) give = 5622 and [M/H] = −0.4. The majority of the literature data agree with these values: $T_{\rm eff}$ = 5600 K and [M/H] = −0.5 dex. Obtaining a suitable fit with these values is difficult, and since the age is greater than the age of the Galaxy, our grid is insufficient. Our data is $T_{\rm eff}$ = 5746 K and [M/H] = −0.35 dex (T. D. Morton et al. 2016). With these values and using $\Delta\nu$=77.2 μHz data, we obtained a model that agrees well with the observations by applying Method DZT: (M, R, Z_0, t_9, $T_{\rm eff}$) = (0.9078, 1.4210, 0.00819, 11.127, 5747). α and Y_0 of this model are 1.5652 and 0.26348, respectively. The observational reference frequencies of this host star are quite uncertain. There are only 5 points on the $\Delta\nu$–ν plot. In the models, $\nu_{\rm min0} \sim 1722$ and $\nu_{\rm min1}$=1126 μHz.

4.12.5 KIC 8866102

Spectroscopic data for this host show significant scatter. In this case, we can apply the MinZ method to KIC 8866102. We calculated the $\Delta\nu$ of this star directly from the frequencies as 84.2 μHz. It is given as 83.6 μHz in the literature. For the MinZ method, χ^2 is computed as in S. Örtel et al. (2025). In Figs 12(a), (b), and (c), log(χ^2) is plotted with respect to M, Z, and log g, respectively. In all of the panels, χ^2 is minimum at a single value of the horizontal axis. According to the MinZ method, (M, Z, log g) = (1.25, 0.0163, 4.263). For a solar-like oscillating star with precise observational asteroseismic data, we obtain a unique model for the host star.

This method is the most effective and consistent among those based on asteroseismic data, provided that the $\nu_{\min}$ values are determined. The disadvantage of using $\nu_{\max}$ as a constraint is that it can only be calculated from scaling relationships. $\Delta\nu$, on the other hand, is more useful because it can be calculated from both model and observational oscillation frequencies. However, in some cases, the average value of $\Delta\nu$ may depend on the frequency range used. $\nu_{\min}$ values, however, can be calculated without resorting to scale relationships, and since there is no average value, there is no problem with choosing the frequency range used. If $\nu_{\min}$ values can be obtained observationally, a unique model that best represents the star can be obtained using this method. The disadvantage of the method is that it requires the construction of numerous models. In this respect, the method needs further development.

4.12.6 TIC 277890728

This star has a high Li abundance, A(Li)=2.65 (E. Delgado Mena et al. 2014). It is located in the region of the HR diagram where L is at its maximum after TAMS. In this case, α becomes irrelevant in the $T_{\rm eff}$ calibration. By changing Y_0, we calibrate both L and $T_{\rm eff}$. In Fig. 13, the evolution traces of three different models constructed with three different Y_0s are plotted in HRD. The model parameters that best match the observed properties of the star are as

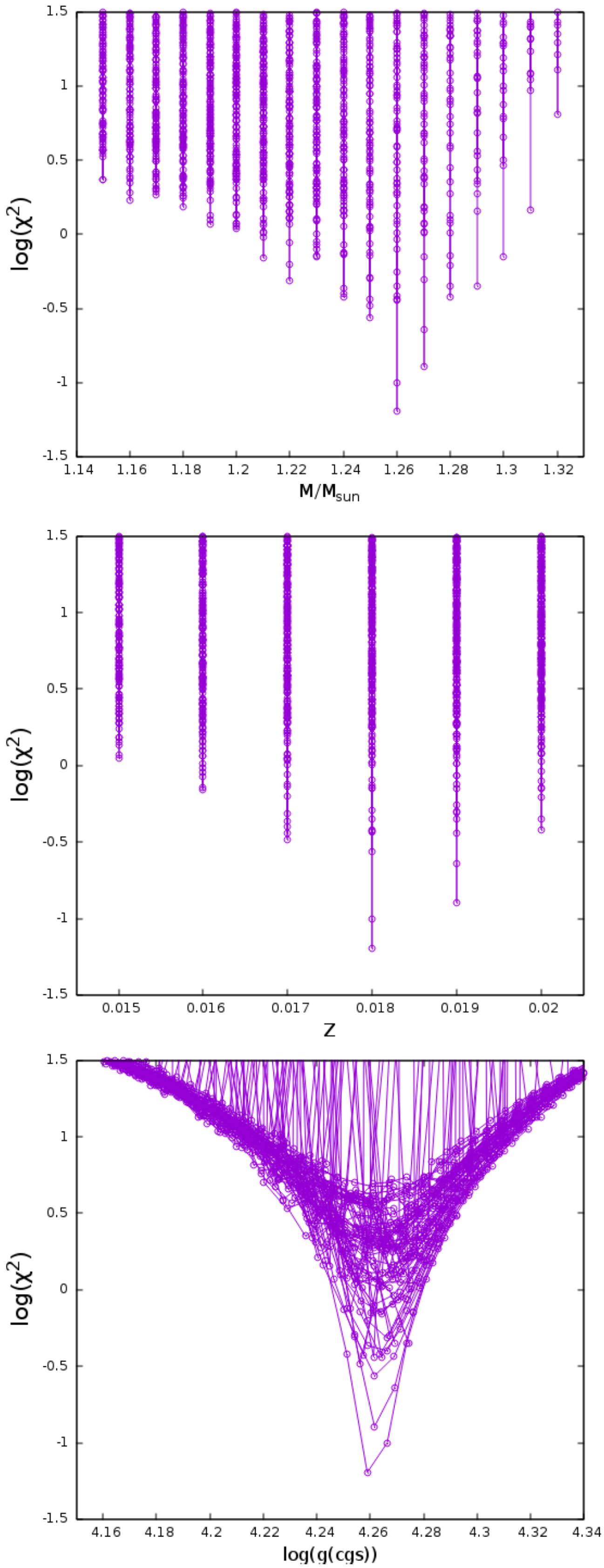

Figure 12. $\log(\chi^2)$ is plotted with respect to M (upper panel), Z (middle panel), and $\log(g)$ (lower panel) for KIC 8866102. For each of the parameters, $\log(\chi^2)$ is minimized at a single point.

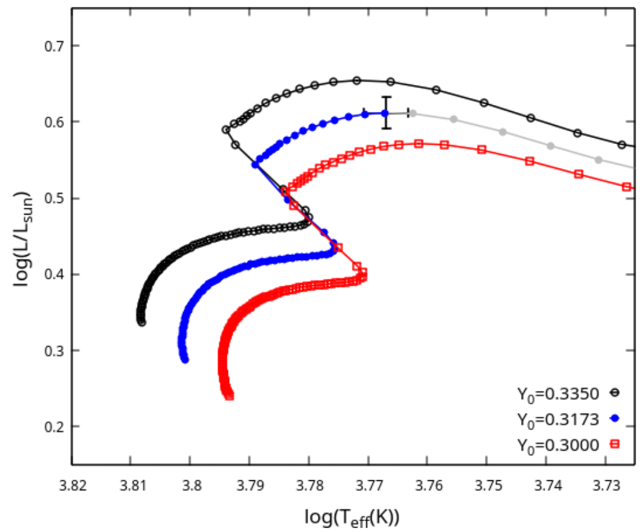

Figure 13. HRD of TIC 277890728 for the three models with different Y_0. The circle, filled circle, and box show the models with Y_0= 0.3350, 0.3173, and 0.3000, respectively. The best model is with Y_0=0.3173.

Table 3. Basic properties of the models constructed for TIC 38828538.

M (M$_\odot$)	R (R$_\odot$)	Z_0	t_9 (Gyr)	$T_{\rm eff}$ (K)
1.1631	4.6914	0.01856	6.7000	4738
1.2800	4.7100	0.01860	4.6600	4787
1.3663	4.9202	0.01868	3.7306	4806
1.4907	5.0431	0.01861	2.8387	4845
1.1394	4.4591	–	–	–

follows: $M = 1.26$ M$_\odot$, $R = 1.97$ R$_\odot$, $Y_0 = 0.3173$, $Z_0 = 0.0319$, and $t_9 = 4.75$ Gyr (see Table A2).

4.12.7 TIC 284181945

The model parameters we obtained by applying the DZTLTeC method are: $(M, R, Z_0, t_9, T_{\rm eff}) = (2.19, 10.33, 0.016, 0.76, 4894)$. The $\Delta\Pi_1$ value for this star was found to be 303.96 ± 0.30 s by W.-X. Lin et al. (2024a). According to $\Delta\nu$ and $\Delta\Pi_1$, TIC 284181945 is an RC star.

4.12.8 TIC 38828538 (HD 29399)

This host is an RGB star (W.-X. Lin et al. 2024a). L is given by C. Pezzotti et al. (2022) as 10.04 L$_\odot$. 3 separate solutions: (1) $L_{\rm mod}$=10.04, (2) $L_{\rm mod}$=11.6681, (3) $T_{\rm eff}$=4845 K (L=12.626 L$_\odot$). $\Delta\Pi_1 = 83.55 \pm 0.09$ s (W.-X. Lin et al. 2024a). The host is an RGB star.

When the difference between $T_{\rm mod}$ and $T_{\rm eff}$ was large, we obtained solutions with different L values to test the uncertainty level in the luminosity. These solutions are listed in Table 3. $T_{\rm mod}$ increases with increasing L. When $L_{\rm mod}$=12.6 L$_\odot$, $T_{\rm mod}$ and $T_{\rm eff}$ are equal. In this case, because the mass increases significantly, there are substantial age differences. The last row of the table shows M and R calculated from corrected scaling relations. $\Delta\nu$ of the model with $M = 1.28$ M$_\odot$ is in good agreement with the observed value. The difference between $T_{\rm mod}$ and $T_{\rm eff}$ is about 58 K for this model.

4.12.9 *TIC 233008631*

TIC 233008631 has the smallest values for $\Delta\nu$ and $\nu_{\rm max}$ among the hosts. For such stars, asteroseismic modelling is complex because the frequencies of only a few modes can be calculated using the ADIPLS package. Therefore, $\Delta\nu$ can only be calculated over a narrow range.

4.12.10 *Habitable planet around KIC 10593626*

This system, located at a distance of 197.5 pc, hosts a super-Earth at an orbital distance of 0.812 au (A. S. Bonomo et al. 2023). This planet, in the habitable zone, has an orbital period of 290 d. According to the model we obtained using the DZT method, the host's Z_0 is 0.0089. The age of the system was found to be 11.25 Gyr. If life had arisen, there would have been plenty of time for it to evolve.

5 CONCLUSIONS

Asteroseismology is essential for understanding the internal structure of stars and constraining their fundamental parameters. Using quantities such as $\Delta\nu$, $\nu_{\rm max}$, and $\delta\nu_{02}$, stellar properties can be determined with much higher precision than with other methods. In recent years, the growing number of solar-like oscillating host stars has further strengthened the link between asteroseismology and exoplanet research, enabling the two fields to advance together.

In this study, we compiled data on 127 host stars (and six candidates) from the literature and constructed interior models of these stars using the MESA code. Rather than applying a single method, we developed multiple approaches based on the available data and their associated uncertainties. We used $\Delta\nu$ and $Z_{\rm s}$ as constraints in all the methods we implemented. Additionally, we included one or more of $\delta\nu_{02}$, $\nu_{\rm min0}$, $\nu_{\rm min1}$, L, $T_{\rm eff}$, or R as constraints in the applied methods, depending on the sensitivity of the data and their compatibility with other data.

Two key results emerged from our models. First, with only a few exceptions, the majority of host stars have a Z_0 greater than 0.007 (Fig. 7). This suggests that the threshold condition for planet formation is $Z_0 \approx 0.007$; if the metallicity of a host star is below this value, no planet formation is observed. Second, the age–metallicity relationship is quite variable. Both old and young stars can be metal-poor. For the most metal-rich stars of their time, the age–metallicity relationship appears linear up to $t_9 = 6$ Gyr. When $t_9 < 6$ Gyr, it seems to remain constant in the range $Z_0 = 0.007$–0.033. These results provide important insights into the chemical evolution of the Galactic disc. To further examine this threshold, we modelled two hosts, TOI-2018 and HD 155358, reported to have very low metallicities, without asteroseismic constraints. Their surface metallicities ($Z_{\rm s} = 0.006$ and 0.004) are below the critical value of $Z_0 \approx 0.007$. By including microscopic diffusion, we show that both stars can be reproduced with $Z_0 = 0.007$. The difference between Z_0 and $Z_{\rm s}$ is smaller in TOI-2018 and larger in HD 155358, reflecting the efficiency of diffusion. These results indicate that low surface metallicities do not necessarily imply low initial metallicities, and are consistent with the proposed threshold.

We also modelled 12 hosts classified as RC stars in the literature, taking into account mass-loss along the red giant branch. We show that mass-loss has a crucial effect on the initial masses and ages of these stars, and may have important consequences for the survival of close-in planets during the RC phase.

For the solar-like oscillating KIC 8866102 with precise observational asteroseismic data ($\Delta\nu$, $\nu_{\rm min0}$, $\nu_{\rm min1}$) and $Z_{\rm s}$, we apply the MinZ method (Fig. 12) developed by S. Örtel et al. (2025). We obtain a unique model for the host star. We could not apply this method to more stars due to the large number of models required.

Another important outcome of this study is the discovery of a relationship between Z_0 and the observed $Z_{\rm s}$ for the hosts. For the input parameter Z_0 used in the models, we derive a useful expression as a function of stellar M, R, and $Z_{\rm s}$. This expression can be used to estimate Z_0 by accounting for the decrease in $Z_{\rm s}$ caused by microscopic diffusion.

The radius of a planet is mainly dependent on its mass. It is known that the incident flux, in particular, has a significant effect on gas giants. When using irradiation energy per gram per second rather than flux, we obtain a one-to-one relationship for the radius. We show for the first time that $R_{\rm p}$ depends not only on $M_{\rm p}$ and l_{-}, but also on one of the orbital parameters (P or a). Interestingly, our expression provides radius predictions for all planets, whether they are hot-Jupiter or terrestrial planets, including non-transiting planets.

This study provides the fundamental parameters of 127 solar-like oscillating host stars and their planets, establishing an essential catalogue in the literature. The *TESS* mission has significantly expanded the sample of evolved stars in the literature, allowing us to study a larger and more diverse sample of solar-like oscillating host stars. These systems serve as natural laboratories for understanding star–planet evolution and for investigating planet formation and disc evolution. The results offer valuable insights into key questions in both asteroseismology and exoplanet research, while laying a solid foundation for future studies.

Extended data for planetary systems are provided in NASA Exoplanet Archive (R. L. Akeson et al. 2013) and TEPCat (J. Southworth 2011). It may be useful to create a continuously updated catalog of planetary systems with solar-like oscillating hosts using machine learning or to add asteroseismic data to existing catalogues.

ACKNOWLEDGEMENTS

This work is supported by the Scientific and Technological Research Council of Turkey (TÜBİTAK: 122F107, 123F019).

DATA AVAILABILITY

The data underlying this article will be shared on reasonable request to the corresponding author.

REFERENCES

Abdurro'uf et al., 2022, ApJS, 259, 35
Adamów M., Niedzielski A., Kowalik K., Villaver E., Wolszczan A., Maciejewski G., Gromadzki M., 2018, A&A, 613, A47
Addison B. C. et al., 2021, MNRAS, 502, 3704
Aguilera-Gómez C., Ramírez I., Chanamé J., 2018, A&A, 614, A55
Aguilera-Gómez C., Jones M. I., Chanamé J., 2023, A&A, 670, A73
Akeson R. L. et al., 2013, PASP, 125, 989
Appourchaux T. et al., 2012, A&A, 543, A54
Arentoft T. et al., 2019, A&A, 622, A190
Asplund M., Grevesse N., Sauval A. J., Scott P., 2009, ARA&A, 47, 481

Baglin A. et al., 2006, in Fridlun M., Baglin A, Lochard J., Conroy L., eds, ESA SP-1306: The CoRoT Mission Pre-Launch Status - Stellar Seismology and Planet Finding, 1306, ESA, Noordwijk, p. 33
Baines E. K., McAlister H. A., ten Brummelaar T. A., Sturmann J., Sturmann L., Turner N. H., Ridgway S. T., 2009, ApJ, 701, 154
Baines E. K., Armstrong J. T., van Belle G. T., 2013, ApJ, 771, L17
Ball W. H. et al., 2020, MNRAS, 499, 6084
Barclay T. et al., 2013, Nature, 494, 452
Batalha N. M. et al., 2011, ApJ, 729, 27
Batalha N. M. et al., 2013, ApJS, 204, 24
Beard C. et al., 2024, AJ, 168, 149
Benedict G. F., McArthur B. E., Nelan E. P., Wittenmyer R., Barnes R., Smotherman H., Horner J., 2022, AJ, 163, 295
Berger T. A., Huber D., Gaidos E., van Saders J. L., 2018, ApJ, 866, 99
Böhm-Vitense E., 1958, Z. Astrophys., 46, 108
Bonfanti A., Ortolani S., Piotto G., Nascimbeni V., 2015, A&A, 575, A18
Bonomo A. S. et al., 2023, A&A, 677, A33
Bonomo A. S. et al., 2025, A&A, 696, A233
Borgniet S. et al., 2014, A&A, 561, A65
Borgniet S., Lagrange A.-M., Meunier N., Galland F., 2017, A&A, 599, A57
Borucki W. J. et al., 2010a, ApJ, 713, L126
Borucki W. J. et al., 2010b, Science, 327, 977
Bouchy F., Bazot M., Santos N. C., Vauclair S., Sosnowska D., 2005, A&A, 440, 609
Bressan A., Marigo P., Girardi L., Salasnich B., Dal Cero C., Rubele S., Nanni A., 2012, MNRAS, 427, 127
Brewer J. M., Fischer D. A., 2018, ApJS, 237, 38
Brewer J. M., Fischer D. A., Valenti J. A., Piskunov N., 2016, ApJS, 225, 32
Brewer J. M., Fischer D. A., Valenti J. A., Piskunov N., 2017, ApJS, 230, 12
Brown T. M., Gilliland R. L., Noyes R. W., Ramsey L. W., 1991, ApJ, 368, 599
Burke C. J. et al., 2014, ApJS, 210, 19
Burrows A., Guillot T., Hubbard W. B., Marley M. S., Saumon D., Lunine J. I., Sudarsky D., 2000, ApJ, 534, L97
Butler R. P. et al., 2006, ApJ, 646, 505
Campante T. L. et al., 2015, ApJ, 799, 170
Campante T. L. et al., 2017, MNRAS, 469, 1360
Campante T. L. et al., 2019, ApJ, 885, 31
Carter J. A. et al., 2012, Science, 337, 556
Casagrande L., Flynn C., Portinari L., Girardi L., Jimenez R., 2007, MNRAS, 382, 1516
Chaplin W. J. et al., 2013, ApJ, 766, 101
Chaplin W. J. et al., 2014, ApJS, 210, 1
Charbonnel C. et al., 2020, A&A, 633, A34
Chavero C., de la Reza R., Ghezzi L., Llorente de Andrés F., Pereira C. B., Giuppone C., Pinzón G., 2019, MNRAS, 487, 3162
Chen R. E., Jiang J. H., Rosen P. E., Fahy K. A., Chen Y., 2023, Galaxies, 11, 112
Christensen-Dalsgaard J., 1988, in Christensen-Dalsgaard J., Frandsen S., eds, Proc. IAU Symp. 123, Advances in Helio- and Asteroseismology. Kluwer, Dordrecht, p. 295
Christensen-Dalsgaard J., 1993, in Brown T,. M., eds, ASP Conf. Proc. Vol. 42, GONG 1992. Seismic Investigation of the Sun and Stars. Astron. Soc. Pac., San Francisco, p. 347
Christensen-Dalsgaard J., 2008, Ap&SS, 316, 113
Cochran W. D., Endl M., Wittenmyer R. A., Bean J. L., 2007, ApJ, 665, 1407
Coughlin J. L. et al., 2016, ApJS, 224, 12
Dai F. et al., 2023, AJ, 166, 49
Davies G. R. et al., 2015, MNRAS, 446, 2959
Davies G. R. et al., 2016, MNRAS, 456, 2183
Dawson R. I., Johnson J. A., 2018, ARA&A, 56, 175
Deheuvels S., Brandão I., Silva Aguirre V., Ballot J., Michel E., Cunha M. S., Lebreton Y., Appourchaux T., 2016, A&A, 589, A93
Deka-Szymankiewicz B., Niedzielski A., Adamczyk M., Adamów M., Nowak G., Wolszczan A., 2018, A&A, 615, A31
Delgado Mena E. et al., 2014, A&A, 562, A92
Delrez L. et al., 2021, Nat. Astron., 5, 775
Di Mauro M. P. et al., 2022, ApJ, 940, 93
Dressing C. D. et al., 2015, ApJ, 800, 135
Dubber S. C. et al., 2019, MNRAS, 490, 5103
Dumusque X. et al., 2014, ApJ, 789, 154
Ezer D., Cameron A. G. W., 1965, Can. J. Phys., 43, 1497
Feng F. et al., 2022, ApJS, 262, 21
Ferguson J. W., Alexander D. R., Allard F., Barman T., Bodnarik J. G., Hauschildt P. H., Heffner-Wong A., Tamanai A., 2005, ApJ, 623, 585
Feuillet D. K., Bovy J., Holtzman J., Girardi L., MacDonald N., Majewski S. R., Nidever D. L., 2016, ApJ, 817, 40
Fischer D. et al., 2009, ApJ, 703, 1545
Forsberg R., Ryde N., Jönsson H., Rich R. M., Johansen A., 2022, A&A, 666, A125
Frasca A. et al., 2016, A&A, 594, A39
Fulton B. J., Petigura E. A., 2018, AJ, 156, 264
Furlan E. et al., 2018, ApJ, 861, 149
Gaia Collaboration, 2018, A&A, 616, A1
Gaia Collaboration, 2021, A&A, 649, A1
Gajdoš P., Vaňko M., Parimucha Š., 2019, Res. Astropart. Astrophys., 19, 041
García Pérez A. E. et al., 2021, MNRAS, 505, 4496
Ghezzi L., Cunha K., Smith V. V., de Araújo F. X., Schuler S. C., de la Reza R., 2010, ApJ, 720, 1290
Ghezzi L., Montet B. T., Johnson J. A., 2018, ApJ, 860, 109
Giguere M. J. et al., 2012, ApJ, 744, 4
Gilliland R. L. et al., 2013, ApJ, 766, 40
Gizon L. et al., 2013, PNAS, 110, 13267
Gonzalez G., Carlson M. K., Tobin R. W., 2010, MNRAS, 403, 1368
González-Álvarez E. et al., 2017, A&A, 606, A51
Goździewski K., Maciejewski A. J., Migaszewski C., 2007, ApJ, 657, 546
Grieves N. et al., 2018, MNRAS, 481, 3244
Grunblatt S. K. et al., 2018, ApJ, 861, L5
Harakawa H. et al., 2015, ApJ, 806, 5
Hatt E. et al., 2023, A&A, 669, A67
Haywood R. D. et al., 2018, AJ, 155, 203
Hekker S., Meléndez J., 2007, A&A, 475, 1003
Hill M. L. et al., 2021, AJ, 162, 211
Hon M. et al., 2023, Nature, 618, 917
Howell S. B. et al., 2014, PASP, 126, 398
Huang C. X. et al., 2018, ApJ, 868, L39
Huber D., 2016, Proc. IAU Symp. 29B, Astronomy in Focus, as presented at the IAU XXIX General Assembly. Kluwer, Dordrecht, p. 620
Huber D., 2018, ASSP, 49, 119
Huber D. et al., 2013a, ApJ, 767, 127
Huber D. et al., 2013b, Science, 342, 331
Huber D. et al., 2019, AJ, 157, 245
Huber D. et al., 2022, AJ, 163, 79
Iglesias C. A., Rogers F. J., 1996, ApJ, 464, 943
Iglesias C. A., Rogers F. J., 1993, ApJ, 412, 752
Jeong G. et al., 2018, A&A, 610, A3
Jeong G., Lee B.-C., Park M.-G., Bang T.-Y., Han I., 2022, A&A, 662, A12
Jermyn A. S. et al., 2023, ApJS, 265, 15
Jiang C. et al., 2020, ApJ, 896, 65
Jiang C. et al., 2023, ApJ, 945, 20
Jofré E., Petrucci R., Saffe C., Saker L., Artur de la Villarmois E., Chavero C., Gómez M., Mauas P. J. D., 2015, A&A, 574, A50
Johnson J. A. et al., 2010, ApJ, 721, L153
Johnson J. A. et al., 2011a, AJ, 141, 16
Johnson J. A. et al., 2011b, ApJS, 197, 26
Jones M. I., Jenkins J. S., Bluhm P., Rojo P., Melo C. H. F., 2014, A&A, 566, A113
Jones M. I., Jenkins J. S., Rojo P., Melo C. H. F., Bluhm P., 2015, A&A, 573, A3
Jones M. I. et al., 2016, A&A, 590, A38
Jones M. I. et al., 2021, A&A, 646, A131
Kane S. R. et al., 2015, ApJ, 806, 60
Kang W., Lee S.-G., Kim K.-M., 2011, ApJ, 736, 87
Kayhan C., Yıldız M., Çelik Orhan Z., 2019, MNRAS, 490, 1509

Kjeldsen H., Bedding T. R., 1995, A&A, 293, 87
Kjeldsen H., Bedding T. R., Christensen-Dalsgaard J., 2008, ApJ, 683, L175
Kunitomo M., Ikoma M., Sato B., Katsuta Y., Ida S., 2011, ApJ, 737, 66
Kuzuhara M. et al., 2013, ApJ, 774, 11
Lebzelter T., Wood P. R., 2011, A&A, 529, A137
Lee B.-C. et al., 2015, A&A, 584, A79
Leleu A. et al., 2023, A&A, 669, A117
Lin D. N. C., Bodenheimer P., Richardson D. C., 1996, Nature, 380, 606
Lin W.-X., Qian S.-B., Zhu L.-Y., 2024a, ApJ, 971, L50
Lin W.-X., Qian S.-B., Zhu L.-Y., Liao W.-P., Li F.-X., 2024b, AJ, 168, 27
Lin W.-X., Qian S.-B., Zhu L.-Y., Liao W.-P., Li F.-X., Shi X.-D., Li L.-J., Zhao E.-G., 2025a, ApJ, 978, 24
Lin W.-X. et al., 2025b, ApJS, 279, 31
Liu Y. J., Tan K. F., Wang L., Zhao G., Sato B., Takeda Y., Li H. N., 2014, ApJ, 785, 94
Lopez E. D., Fortney J. J., 2016, ApJ, 818, 4
Luck R. E., 2017, AJ, 153, 21
Luhn J. K., Bastien F. A., Wright J. T., Johnson J. A., Howard A. W., Isaacson H., 2019, AJ, 157, 149
Lund M. N. et al., 2017, ApJ, 835, 172
Lundkvist M. S., Huber D., Silva Aguirre V., Chaplin W. J., 2018, preprint (arXiv:1804.02214)
Luque R. et al., 2019, A&A, 631, A136
Mahdi D., Soubiran C., Blanco-Cuaresma S., Chemin L., 2016, A&A, 587, A131
Maldonado J., Villaver E., 2016, A&A, 588, A98
Marcy G. W. et al., 2014, ApJS, 210, 20
Marmier M. et al., 2013, A&A, 551, A90
Meléndez J. et al., 2008, A&A, 484, L21
Ment K., Fischer D. A., Bakos G., Howard A. W., Isaacson H., 2018, AJ, 156, 213
Meschiari S., Laughlin G., Vogt S. S., Butler R. P., Rivera E. J., Haghighipour N., Jalowiczor P., 2011, ApJ, 727, 117
Metcalfe T. S. et al., 2012, ApJ, 748, L10
Metcalfe T. S. et al., 2023, AJ, 166, 167
Miglio A. et al., 2012, MNRAS, 419, 2077
Miglio A. et al., 2021, A&A, 645, A85
Mills S. M. et al., 2019, AJ, 157, 145
Montes D. et al., 2018, MNRAS, 479, 1332
Morton T. D., Bryson S. T., Coughlin J. L., Rowe J. F., Ravichandran G., Petigura E. A., Haas M. R., Batalha N. M., 2016, ApJ, 822, 86
Naef D., Mayor M., Pepe F., Queloz D., Santos N. C., Udry S., Burnet M., 2001, A&A, 375, 205
Niedzielski A. et al., 2015, A&A, 573, A36
Niedzielski A. et al., 2016, A&A, 588, A62
Nielsen M. B. et al., 2020, A&A, 641, A25
O'Connor C. E., Bildsten L., Cantiello M., Lai D., 2023, ApJ, 950, 128
Örtel S., Yıldız M., Çelik Orhan Z., 2025, MNRAS, 538, 844
O'Toole S. et al., 2009, ApJ, 697, 1263
Ortiz M. et al., 2016, A&A, 595, A55
Ottoni G. et al., 2022, A&A, 657, A87
Pál A. et al., 2008, ApJ, 680, 1450
Paletou F., Böhm T., Watson V., Trouilhet J.-F., 2015, A&A, 573, A67
Paquette C., Pelletier C., Fontaine G., Michaud G., 1986, ApJS, 61, 177
Pasquini L., Bonifacio P., Randich S., Galli D., Gratton R. G., 2004, A&A, 426, 651
Paxton B., Bildsten L., Dotter A., Herwig F., Lesaffre P., Timmes F., 2011, ApJS, 192, 35
Paxton B. et al., 2013, ApJS, 208, 42
Paxton B. et al., 2015, ApJS, 220, 15
Paxton B. et al., 2018, ApJS, 234, 34
Paxton B. et al., 2019, ApJS, 243, 10
Perdelwitz V., Trifonov T., Teklu J. T., Sreenivas K. R., Tal-Or L., 2024, A&A, 683, A125
Petigura E. A. et al., 2017, AJ, 154, 107
Pezzotti C. et al., 2022, A&A, 657, A89
Philipot F., Lagrange A.-M., Kiefer F., Rubini P., Delorme P., Chomez A., 2023, A&A, 678, A107
Pinsonneault M. H. et al., 2018, ApJS, 239, 32
Planck Collaboration VI, 2020, A&A, 641, A6
Rajpaul V. M. et al., 2021, MNRAS, 507, 1847
Reimers D., 1975, MSRSL, 8, 369
Rice M., Brewer J. M., 2020, ApJ, 898, 119
Ricker G. R. et al., 2015, JATIS, 1, 014003
Rosenthal L. J. et al., 2021, ApJS, 255, 8
Rowe J. F. et al., 2014, ApJ, 784, 45
Safonova M., Murthy J., Shchekinov Y. A., 2016, Int. J. Astrobiol., 5, 93
Salaris M., Chieffi A., Straniero O., 1993, ApJ, 414, 580
Santos N. C., Israelian G., Mayor M., 2004, A&A, 415, 1153
Santos N. C. et al., 2013, A&A, 556, A150
Sato B. et al., 2008, PASJ, 60, 1317
Sato B. et al., 2013, ApJ, 762, 9
Saunders N. et al., 2025, AJ, 169, 75
Sayeed M., Huber D., Chontos A., Li Y., 2025, AJ, 170, 212
Seager S., Mallén-Ornelas G., 2003, ApJ, 585, 1038
Setiawan J. et al., 2005, A&A, 437, L31
Sharma S., Stello D., Bland-Hawthorn J., Huber D., Bedding T. R., 2016, ApJ, 822, 15
Silva Aguirre V. et al., 2015, MNRAS, 452, 2127
Soto M. G., Jones M. I., Jenkins J. S., 2021, A&A, 647, A157
Soubiran C., Brouillet N., Casamiquela L., 2022, A&A, 663, A4
Sousa S. G. et al., 2008, A&A, 487, 373
Sousa S. G. et al., 2015, A&A, 576, A94
Sousa S. G. et al., 2018, A&A, 620, A58
Southworth J., 2011, MNRAS, 417, 2166
Stassun K. G., Collins K. A., Gaudi B. S., 2017, AJ, 153, 136
Stock S., Reffert S., Quirrenbach A., 2018, A&A, 616, A33
Tassoul M., 1980, ApJS, 43, 469
Tautvaišienė G. et al., 2022, ApJS, 259, 45
Teng H.-Y. et al., 2022, PASJ, 74, 92
Teng H.-Y. et al., 2022, PASJ, 74, 1309
Teng H.-Y. et al., 2023, PASJ, 75, 1030
Thompson S. E. et al., 2018, ApJS, 235, 38
Ting Y.-S., Conroy C., Rix H.-W., Cargile P., 2019, ApJ, 879, 69
Tognelli E., Dell'Omodarme M., Valle G., Prada Moroni P. G., Degl'Innocenti S., 2021, MNRAS, 501, 383
Trifonov T. et al., 2022, AJ, 164, 156
Tsantaki M., Sousa S. G., Santos N. C., Montalto M., Delgado-Mena E., Mortier A., Adibekyan V., Israelian G., 2014, A&A, 570, A80
Valizadegan H. et al., 2022, ApJ, 926, 120
Van Eylen V. et al., 2014, ApJ, 782, 14
Van Eylen V. et al., 2015, in García R. A., Ballot J., eds, Proc. CoRoT Symposium 3/Kepler KASC-7 Joint Meeting, Vol. 101. EPJ Web Conf., p. A02005
Venner A., Vanderburg A., Pearce L. A., 2021, AJ, 162, 12
Vernekar N., Lucatello S., Bragaglia A., Miglio A., Sanna N., Andreuzzi G., Frasca A., 2024, A&A, 684, A85
Villaver E., Livio M., 2007, ApJ, 661, 1192
Villaver E., Livio M., 2009, ApJ, 705, L81
Wang L. et al., 2016, AJ, 152, 6
Weeks A. et al., 2025, MNRAS, 541, 2459
Weiss L. M. et al., 2024, ApJS, 270, 8
Wilson R. F. et al., 2022, AJ, 163, 128
Wittenmyer R. A., Endl M., Cochran W. D., Levison H. F., Henry G. W., 2009, ApJS, 182, 97
Wittenmyer R. A., Endl M., Wang L., Johnson J. A., Tinney C. G., O'Toole S. J., 2011, ApJ, 743, 184
Wittenmyer R. A., Liu F., Wang L., Casagrande L., Johnson J. A., Tinney C. G., 2016, AJ, 152, 19
Wittenmyer R. A. et al., 2016, ApJ, 818, 35
Wittenmyer R. A., Jones M. I., Zhao J., Marshall J. P., Butler R. P., Tinney C. G., Wang L., Johnson J. A., 2017a, AJ, 153, 51
Wittenmyer R. A. et al., 2017b, AJ, 154, 274
Xiao G.-Y. et al., 2023, RAA, 23, 055022
Xie J.-W., 2014, ApJS, 210, 25
Yıldız M., 2015, RAA, 15, 2244

Yıldız M., 2023, MNRAS, 518, 5552
Yıldız M., Kızıloğlu N., 1997, A&A, 326, 187
Yıldız M., Çelik Orhan Z., Kayhan C., Turkoglu G. E., 2014, MNRAS, 445, 4395
Yıldız M., Çelik Orhan Z., Kayhan C., 2016, MNRAS, 462, 1577
Yıldız M., Örtel S., Çakır Alsaç T., 2026, MNRAS, 549, stag1069
Zhang J., Qian S.-B., Wu Y., Zhou X., 2019, ApJS, 244, 43
Zhang J. et al., 2021, AJ, 162, 89
Zhang L.-y., Su T., Misra P., Han X. L., Meng G., Pi Q., Yang J., 2023, ApJS, 264, 17
Zhou J. et al., 2024, ApJS, 271, 17

APPENDIX A: BASIC ASTEROSEISMIC AND NON-ASTEROSEISMIC PROPERTIES OF *Kepler* AND *TESS* TARGETS

Table A1. Observationalphysical properties of solar-like oscillating host stars and their planets. The columns are as follows, in order: host ID, effective temperature ($T_{\rm eff}$), host mass (M) and radius (R), luminosity (L), metallicity ([M/H]), large separation ($\Delta\nu$), frequency of maximum amplitude ($\nu_{\rm max}$), small separation ($\delta\nu_{02}$), reference frequencies ($\nu_0 = \nu_{\rm min0}$ and $\nu_1 = \nu_{\rm min1}$), distance (d), semimajor axis (a), orbital period (P), planet radius ($R_{\rm p}$), and mass ($M_{\rm p}$). The final column lists the references.

Host	$T_{\rm eff}$(K)	M(M$_\odot$)	R (R$_\odot$)	L (L$_\odot$)	[M/H]	$\Delta\nu$ (μHz)	$\nu_{\rm max}$ (μHz)	$\delta\nu_{02}$ (μHz)	ν_0 (μHz)	ν_1 (μHz)	d (pc)	a (AU)	P (day)	$R_{\rm p}$ (R$_{\rm J}$)	$M_{\rm p}$ (M$_{\rm J}$)	Ref
KIC 3544595	5669 ± 75	0.91± 0.03	0.92± 0.01	0.78± 0.02	−0.18± 0.01	145.77± 0.45	3366.0 ± 81.0	8.6 ± 1.7	3283.2	2701.9	96.0	0.053	4.727	0.1319	0.0126	3,5,6,9,**79**
KIC 3632418	6148 ± 111	1.41± 0.03	1.90± 0.02	4.87± 0.03	−0.19± 0.21	60.90± 0.40	1159.0 ± 44.0	4.3 ± 0.7	1422.1	1065.2	108.5	0.043	2.786	0.1462	0.024	6,8,9,**36**,201
KIC 4141376	6148 ± 71	1.03± 0.04	1.03± 0.02	1.33± 0.01	−0.24± 0.05	128.80± 1.30	2928.0 ± 97.0	–	–	–	214.4	0.103	11.873	0.1974	0.0160	5,9,**10**
KIC 4143755	5746 ± 66	0.91± 0.06	1.41± 0.06	1.93± 0.03	−0.35± 0.09	77.20± 1.30	1458.0 ± 57.0	–	1504.7	1272.7	385.7	0.135	19.56	0.220	–	5,9,**11**,**37**
KIC 4349452	6270 ± 79	1.17± 0.03	1.32± 0.02	2.46± 0.03	−0.04± 0.10	98.27± 0.57	2106.0 ± 50.0	7.8 ± 1.6	2365.2	1884.5	241.2	0.068	6.239	0.2452	0.0275	5,6,9,**82**,201
KIC 4914423	5845 ± 88	1.21± 0.03	1.49± 0.24	2.36± 0.05	0.07± 0.11	81.50± 1.60	1663.0 ± 56.0	–	1827.3	1581.1	506.3	0.133	15.965	0.311	0.0370	3,5,9,**83**,202
KIC 5094751	5952 ± 75	1.09± 0.09	1.39± 0.02	2.07± 0.04	−0.08± 0.10	91.10± 2.30	1745.0 ± 117.0	–	–	–	477.7	0.070	6.500	0.2220	0.015	3,5,9,**36**,203
KIC 5866724	6169 ± 50	1.25± 0.02	1.44± 0.03	2.83± 0.04	0.09± 0.08	89.56± 0.48	1880.0 ± 60.0	7.6 ± 1.2	2261.4	1698.3	301.4	0.035	2.155	0.1288	0.0076	5,9,**37**,**82**,201
KIC 6196457	5871 ± 94	1.21± 0.08	1.70± 0.05	–	0.17± 0.11	66.60± 1.10	1299.0 ± 53.0	–	–	1123.0	481.3	0.122	13.749	0.3130	0.2020	5,9,**37**,**84**
KIC 6278762	5046 ± 74	0.76± 0.04	0.75± 0.01	0.37	−0.55± 0.07	179.64± 0.76	4538.0 ± 144.0	–	4220.8	3411.7	36.6	0.042	3.600	0.0360	–	1,6,9,**85**
KIC 6448890	4840 ± 97	1.32± 0.13	4.23± 0.15	8.03± 0.36	0.20± 0.16	17.40± 0.24	244.30 ± 3.4	–	–	–	929.8	0.103	10.502	0.5810	0.0700	9,**140**,141,148
KIC 6521045	5825 ± 75	1.08± 0.06	1.49± 0.04	2.51± 0.03	0.02± 0.10	77.00± 1.10	1502.0 ± 31.0	5.3 ± 0.5	1643.2	1259.1	307.0	0.073	6.887	0.1180	0.023	1,**3**,6,9
KIC 7277317	4812 ± 41	1.15± 0.12	2.69± 0.11	3.01± 0.16	0.14± 0.04	33.00± 0.72	533.00 ± 15	–	–	–	1092.4	0.126	16.339	1.1400	1.0100	9,110,136,**137**,**138**,141
KIC 7670943	6463 ± 110	1.30± 0.07	1.46± 0.09	–	−0.11± 0.01	88.60± 1.30	1895.0 ± 73.0	–	2191.4	1694.4	293.9	–	18.012	0.1532	–	5,88,**89**,201,232
KIC 8077137	6072 ± 75	1.18± 0.07	1.66± 0.04	3.61± 0.06	−0.09± 0.10	68.80± 0.64	1324.0 ± 39.0	5.6 ± 1.0	1494.3	1140.0	397.9	0.125	15.090	0.1268	0.0119	5,9,**37**,**90**,205
KIC 8292840	6212 ± 100	1.18± 0.06	1.35± 0.04	2.75± 0.03	−0.21± 0.10	92.85± 0.35	1983.0 ± 37.0	7.8 ± 1.3	245.6	1730.6	231.2	–	10.50	0.131	–	5,6,9,**11**,237
KIC 8349582	5652	1.08± 0.08	1.41± 0.04	1.85± 0.04	0.220	83.60± 1.40	1677.0 ± 90.0	–	–	–	453.4	0.102	11.523	0.3050	0.0410	**3**,5,9,**37**,202
KIC 8478994	5342	0.80± 0.07	0.77± 0.03	0.48± 0.01	−0.2954	178.70± 1.40	–	–	–	3849.0	64.0	0.100	13.367	0.0270	–	5,9,**91**,201
KIC 8494142	6144 ± 106	1.32± 0.10	1.85± 0.05	4.32± 0.11	0.13± 0.10	61.80± 0.76	1113.0 ± 81.0	–	–	1028.6	557.9	0.173	23.000	0.2360	0.1167	5,**37**,**84**,88
KIC 8866102	6325 ± 75	1.21± 0.03	1.35± 0.01	2.85± 0.02	0.01± 0.10	94.50± 0.60	2014.0 ± 32.0	8.0 ± 1.7	2470.0	1801.0	132.0	0.123	17.834	0.2532	–	6,**93**,209
KIC 9592705	6174 ± 92	1.45± 0.15	2.09± 0.15	–	0.22± 0.10	53.50± 0.30	1008.0 ± 21.0	4.9 ± 1.2	1265.4	971.0	436.3	–	10.275	0.2912	–	5,6,7,**89**,232
KIC 9955598	5460 ± 75	0.91± 0.05	0.90± 0.01	0.63± 0.01	0.08± 0.10	153.18± 0.14	3546.0 ± 119.0	9.0 ± 0.8	3606.2	2842.8	68.1	0.319	68.958	0.1069	0.019	5,9,**36**,221
KIC 10585852	4997 ± 37	1.25± 0.19	3.42± 0.26	7.19± 0.43	0.01± 0.03	23.49± 0.19	350.5 ± 2.6	–	–	–	1267.4	–	8.575	0.367	–	9,**11**,136,141
KIC 10586004	5770 ± 83	1.18± 0.03	1.65± 0.01	2.85± 0.05	0.29± 0.10	69.20± 1.40	1395.0 ± 40.0	–	1556.9	1070.3	415.8	0.130	15.800	0.2140	0.06	5,9,88,**94**
KIC 10593626	5642 ± 50	0.86± 0.05	0.87± 0.01	0.64± 0.01	−0.27± 0.08	137.50± 1.40	–	–	–	–	197.5	0.812	289.864	0.1870	0.0290	5,9,**36**,141
KIC 10666592	6350 ± 80	1.47± 0.08	1.84± 0.23	6.18± 0.08	0.26± 0.08	59.22± 0.59	–	–	1569.2	1182.2	333.4	0.038	2.205	1.3600	1.7800	5,9,**95**
KIC 10963065	6104 ± 74	1.08± 0.07	1.23± 0.03	1.93± 0.01	−0.20± 0.10	102.90	2071.0	–	2338.8	1817.5	89.1	0.036	2.465	0.0732	–	**3**,9,108
KIC 11295426	5793 ± 74	1.06± 0.02	1.26± 0.01	1.65± 0.01	0.12± 0.07	101.51± 0.09	2154.0 ± 13.0	5.6 ± 0.8	2212.0	1767.4	144.3	0.061	5.399	0.2103	0.0253	6,9,**36**,96
KIC 11401755	5911 ± 66	1.07± 0.04	1.63± 0.02	3.13± 0.07	−0.20± 0.06	67.90± 1.20	1250.0 ± 44.0	5.2 ± 1.4	1371.0	1100.9	539.7	0.115	13.840	0.1329	0.0136	5,9,**97**
KIC 11673802	4921 ± 33	1.11± 0.18	3.39± 0.28	5.17± 0.45	0.11± 0.03	21.42± 0.37	319.3 ± 2.7	–	–	–	1178.7	–	5.288	0.560	–	9,**11**,136,141
KIC 11807274	6225 ± 66	1.24± 0.05	1.58± 0.02	3.34± 0.04	0.03± 0.06	75.71± 0.31	1496.0 ± 56.0	8.1 ± 1.3	1680.9	1334.7	252.2	0.077	7.813	0.1530	–	5,9,**98**
KIC 11853905	5857 ± 120	1.22± 0.05	1.49± 0.07	2.51± 0.05	0.17± 0.06	74.40± 1.10	1436.0 ± 42.0	–	–	–	550.0	0.046	3.214	0.3570	0.0770	5,9,**109**
KIC 11904151	5627 ± 44	0.91± 0.02	1.07± 0.01	1.13± 0.01	−0.15± 0.04	118.20± 0.20	2730.0 ± 280.0	–	2528.2	2528.2	173.0	0.017	0.837	0.1311	0.0102	5,9,99,**100**,212,233
KIC 12069449	5750 ± 50	1.07± 0.02	1.16± 0.03	1.7± 0.04	0.05± 0.02	116.90± 1.20	2561.0	6.5 ± 0.4	2626.2	–	21.1	1.676	799.450	–	1.7520	9,**21**,149,150
TIC 612908	4973 ± 29	1.42± 0.11	4.40	12.34± 0.08	−0.14± 0.02	13.28± 0.60	170.4 ± 5.1	–	–	–	131.6	1.850	847.000	1.2280	1.5470	9,**14**,110,141,217
TIC 1713457	4999 ± 10	1.38± 0.11	4.9± 0.08	14.15± 0.16	−0.09± 0.02	14.17± 0.13	183.1 ± 5.9	–	–	–	73.3	1.333	452.800	–	1.9900	9,49,110,**114**,141
TIC 12723961	5065 ± 75	1.42± 0.07	5.27	11.55± 0.08	−0.10± 0.10	16.25± 0.19	226.6 ± 9.4	–	–	–	111.5	1.190	380.700	–	2.3900	9,**14**,31,236
TIC 13105061	4300 ± 50	1.45± 0.10	16.21± 4.01	27.02± 0.6	−0.07± 0.16	3.79± 0.11	34.1 ± 1.8	–	–	–	474.3	0.422	101.540	–	10.7800	9,110,**115**,141
TIC 17554529	4950 ± 22	2.46± 0.07	12.06± 0.16	**78.16**± 2.76	0.15± 0.02	5.00± 0.01	56.4 ± 1.1	–	–	–	44.7	1.878	585.820	–	7.100	9,**17**,110,**113**,141
TIC 20537900	4934 ± 50	1.28± 0.05	4.96	12.33± 0.14	−0.12± 0.05	13.82± 0.44	172.8 ± 4.3	–	–	–	125.4	1.880	858.000	–	1.7680	9,**14**,72,110,141
TIC 28763463	4894 ± 21	1.10± 0.13	11.16± 0.45	61.66 ± 6.73	−0.14± 0.02	4.86± 0.23	41.3 ± 3.9	–	–	–	116.2	0.950	283.800	–	0.4500	9,72,110,**117**
TIC 38828538	4845 ± 52	1.36± 0.06	4.50± 0.11	–	0.14± 0.03	14.71± 0.06	195.6 ± 0.7	–	–	–	44.0	1.913	892.700	–	1.57	9,22,**142**
TIC 46310554	4867 ± 50	1.22± 0.02	3.40	5.74± 0.05	0.27± 0.05	24.30± 0.29	365.7 ± 5.5	–	–	–	85.1	1.032	341.200	–	1.0000	9,**14**,110,68,141
TIC 48237215	4826 ± 55	1.44± 0.05	5.20± 0.06	12.81± 0.12	0.21± 0.10	13.66± 0.03	182.9 ± 1.6	–	–	–	20.5	1.800	735.100	–	1.9400	9,**30**,102
TIC 49430557	4788 ± 75	1.88± 0.32	11.22± 3.15	63.1± 41.62	−0.08± 0.03	4.53± 0.43	45.1 ± 2.9	–	–	–	54.5	1.180	385.200	–	0.5100	9,110,**117**,118
TIC 53178442	5020 ± 60	1.37± 0.27	4.75	10.31± 0.13	−0.15± 0.06	18.61± 1.37	259.1 ± 7.6	–	–	–	139.3	1.110	362.500	–	1.2700	9,**14**,68,110,141
TIC 53873088	4929 ± 32	1.73± 0.09	5.91± 0.14	14.83± 0.07	0.04± 0.01	12.35± 0.15	169.5 ± 0.6	–	–	–	58.6	1.974	768.700	–	1.4210	9,**17**,24,**30**,55
TIC 57983992	4915	1.31± 0.11	3.49± 0.22	8.32± 0.05	0.22± 0.05	20.44± 0.10	311.3 ± 11.9	–	–	–	88.1	1.492	577.200	–	0.9340	9,**34**,38,104
TIC 63905972	4959 ± 25	1.74	5.03± 0.13	13.77± 0.06	0.01± 0.04	14.58± 0.10	201.4 ± 11.8	–	–	–	55.1	1.129	371.740	–	1.9860	9,**17**,38,105
TIC 68418284	4953 ± 42	2.07± 0.17	–	48.98± 0.34	0.11± 0.03	6.67± 0.12	78.2 ± 3.5	–	–	–	149.3	2.794	1079.557	–	5.8880	9,**12**,101,110,141
TIC 71099944	4840 ± 110	2.00± 0.08	8.56± 0.33	40.31± 0.23	−0.20± 0.10	6.20± 0.10	68.4 ± 2.4	–	–	–	116.5	1.400	578.600	–	2.7000	9,38,**106**,213

Table A1 – *continued*

Host	$T_{\rm eff}$(K)	M(M$_\odot$)	R (R$_\odot$)	L (L$_\odot$)	[M/H]	$\Delta\nu$ (μHz)	$\nu_{\rm max}$ (μHz)	$\delta\nu_{02}$ (μHz)	ν_0 (μHz)	ν_1 (μHz)	d (pc)	a (AU)	P (day)	$R_{\rm p}$ (R$_{\rm J}$)	$M_{\rm p}$ (M$_{\rm J}$)	Ref
TIC 71345433	4940 ± 60	1.55± 0.12	5.13	20.66± 0.47	−0.06± 0.06	10.27± 0.21	124.0 ± 5.8	–	–	–	161.7	1.820	766.000	–	3.4000	9,**14**,68,110,141
TIC 77481104	4794 ± 50	1.51± 0.23	5.01	28.57± 0.46	0.08± 0.03	8.32± 0.65	95.1 ± 4.6	–	–	–	200.5	1.167	400.500	–	1.6150	9,**14**,110,119,141
TIC 82604982	4649 ± 30	1.08± 0.14	8.95± 1.45	54.32± 4.32	−0.22± 0.08	4.04± 0.22	37.8 ± 1.3	–	–	–	687.4	0.576	153.220	–	1.0610	9,**33**,38,107
TIC 95361265	4806 ± 15	1.30± 0.09	6.85± 1.38	43.69± 3.02	−0.20± 0.08	3.89± 0.28	32.9 ± 2.2	–	–	–	748.2	0.690	198.400	–	2.5000	9,**107**,110,120,141
TIC 95473936	5439 ± 44	1.09± 0.02	1.94± 0.05	3.07± 0.01	−0.09± 0.03	53.67± 0.69	939.2 ± 19.5	–	–	–	18.1	0.481	116.688	–	7.4000	9,**14**,38,**77**,214
TIC 111947706	4840± 100	1.63± 0.22	–	15.85± 0.06	0.00± 0.10	11.17± 0.09	128.1 ± 3.2	–	–	–	64.0	0.482	88.876	–	1.5680	9,**12**,38,76,215
TIC 113329742	5011 ± 100	1.43± 0.06	4.86± 0.55	13.09± 3.31	−0.14± 0.10	12.53± 0.17	157.1 ± 4.2	–	–	–	61.4	0.940	286.600	–	0.3100	9,110,121,**122**
TIC 117905020	5264 ± 19	0.98± 0.05	–	4.57± 0.16	−0.28	37.41± 1.08	580.3 ± 11.4	–	–	–	62.9	2.293	1146.600	–	6.1000	9,**57**,110,123
TIC 122555698	5829 ± 80	1.16± 0.03	–	2.77± 0.01	0.10± 0.08	69.00	1280.0	–	–	–	25.4	0.140	17.240	–	0.0696	9,75,**145**
TIC 129649472	4618 ± 113	1.23± 0.15	–	44.48± 0.50	0.17± 0.07	4.10± 0.14	31.6 ± 3.2	–	–	–	78.9	0.810	184.200	–	8.2000	9,31,**32**,81
TIC 136916387	5664 ± 61	0.83± 0.07	1.06± 0.02	1.03± 0.03	**-0.24**± 0.05	122.17± 1.62	2810.0 ± 124.0	–	–	–	14.7	**0.096**	11.5800	**0.1485**	**0.0149**	9,141,**146**,235
TIC 137810576	4985	1.68± 0.11	4.40± 0.10	11.18± 0.06	0.19± 0.04	17.89± 0.14	274.1 ± 8.3	–	–	–	122.4	0.081	6.495	–	0.9600	9,38,68,**74**
TIC 138764379	4798	1.11	4.20	9.84± 0.08	0.13	15.01± 0.09	208.7 ± 4.0	–	–	–	97.2	2.740	1576.000	–	1.2600	9,**14**,38,72,73
TIC 146264536	4842 ± 41	1.75± 0.11	–	29.51± 0.55	0.05± 0.03	7.67± 0.33	89.6 ± 3.0	–	–	–	75.2	2.480	1191.000	–	2.8500	9,**57**,101,110
TIC 148153804	4847 ± 33	1.38± 0.06	5.77± 0.53	10.54± 0.05	0.23± 0.03	14.54± 0.13	194.6 ± 3.9	–	–	–	78.5	2.100	822.300	–	2.4000	9,72,110,**124**,141
TIC 148680230	4891 ± 35	1.53± 0.08	5.52	20.06± 0.21	0.02± 0.03	10.62± 0.54	131.0 ± 6.0	–	–	–	142.7	1.980	841.000	–	1.2300	9,**14**,50,110,141
TIC 156942082	4857 ± 25	1.16± 0.07	10.06± 0.86	54.28± 0.5	0.05± 0.03	6.51± 0.36	62.4 ± 3.1	–	–	–	138.2	0.680	157.570	–	1.6100	9,**24**,72,110,141
TIC 160224839	4686 ± 92	1.49± 0.06	11.12± 1.23	57.46± 0.53	**-0.27**± 0.05	3.13± 0.13	26.0 ± 1.0	–	–	–	100.7	0.715	199.680	–	5.5590	9,**17**,110,141,228
TIC 165722603	4504 ± 62	1.54± 0.09	11.79± 0.24	66.08± 0.73	0.03± 0.08	4.02± 0.02	38.4 ± 0.5	–	–	–	30.7	1.453	510.854	–	11.8200	9,55,110,**126**,141
TIC 169397663	5049 ± 41	1.37± 0.07	4.17± 0.07	9.94± 0.07	0.03± 0.03	18.70± 0.12	264.2 ± 5.1	–	–	–	120.9	1.074	330.000	–	1.2600	9,110,**127**,141,217
TIC 169534187	4861 ± 100	1.47± 0.08	5.51± 0.13	14.90± 0.08	0.27± 0.09	12.66± 0.12	166.0 ± 1.2	–	–	–	105.3	1.501	551.400	–	1.7260	9,**24**,**30**,71
TIC 176379354	5861 ± 44	1.22± 0.04	1.64± 0.06	2.92± 0.01	0.24± 0.04	74.79± 0.34	1402.0 ± 28.7	–	–	–	26.1	2.300	1157.000	–	1.2900	9,38,57,**70**
TIC 198079199	4961 ± 28	1.46± 0.01	–	7.09± 0.03	0.26± 0.07	21.29± 0.05	327.6 ± 14.2	–	–	–	18.4	1.271	428.100	–	1.5600	9,38,55,**69**
TIC 200093173	5601	0.98± 0.13	–	6.91± 0.02	0.32± 0.06	37.71± 1.47	582.6 ± 22.3	–	–	–	42.4	0.115	14.310	–	0.6500	9,**12**,35,38,67
TIC 200723869	6075 ± 90	1.41± 0.05	1.87± 0.03	–	0.19± 0.10	61.40± 1.50	1118.0 ± 40.0	–	–	–	76.9	0.152	18.388	0.6390	0.1380	9,**28**
TIC 201175570	4700 ± 100	1.07± 0.05	4.10± 0.06	–	0.25± 0.10	16.53± 0.02	218.5 ± 2.2	–	–	–	442.3	–	9.691	1.0200	0.3600	**27**
TIC 224312054	4595 ± 76	1.71± 0.07	–	66.52± 0.57	0.19± 0.05	4.17± 0.08	40.3 ± 1.4	–	–	–	113.5	2.949	1124.791	–	19.8710	**12**,50,110,141
TIC 225884682	4891 ± 50	1.28± 0.11	4.53± 0.05	–	−0.01± 0.05	14.27± 0.01	179.7 ± 4.2	–	–	–	82.1	2.020	926.400	–	1.7900	9,**26**
TIC 231019255	4643 ± 35	1.28± 0.06	7.18± 0.03	20.37± 0.14	−0.10± 0.04	7.01± 0.17	72.6 ± 0.9	–	–	–	153.9	2.800	1585.000	–	5.7000	9,**57**,72,110,128
TIC 232074535	4970 ± 70	1.91± 0.21	10.09± 0.32	68.96± 0.87	−0.21± 0.10	4.97± 0.05	55.0 ± 3.4	–	–	–	67.8	1.930	711.000	–	6.5400	9,**25**,38,141
TIC 232620788	5522	1.09	1.76	2.63± 0.01	0.21	59.12± 2.26	1084.6 ± 23.9	–	–	–	67.8	0.362	75.220	–	0.7836	9,**14**,34,38,65
TIC 233008631	4205	0.79± 0.32	16.20± 0.40	96.00± 1.00	−0.07	1.79± 0.05	10.4 ± 1.7	–	–	–	141.5	1.400	562.000	–	2.4000	9,110,**128**,210
TIC 236339228	4745 ± 50	1.90± 0.30	9.90± 0.50	49.97± 0.27	−0.21± 0.05	4.32± 0.14	34.8 ± 2.6	–	–	–	135.3	0.762	176.130	–	2.9000	9,**17**,110,129,141
TIC 246937460	4855 ± 50	1.51± 0.06	–	56.12± 0.48	−0.15± 0.06	4.05± 0.32	36.3 ± 3.2	–	–	–	142.0	5.150	2744.000	–	14.9000	9,**17**,**57**,72,110,141
TIC 247119634	4494 ± 30	1.63± 0.21	13.20± 0.30	66.32± 0.69	0.09± 0.02	4.02± 0.36	37.6 ± 2.7	–	–	–	89.3	1.086	299.360	–	6.9200	9,110,**130**,141,210
TIC 257005016	4847 ±**100**	1.51± 0.06	10.73± 0.14	**52.48**± 0.37	−0.22	4.76± 0.04	50.8 ± 2.4	–	–	–	163.2	0.490	93.400	–	1.6500	9,**24**,38,**226**
TIC 261136679	6037 ± 45	1.09± 0.03	–	1.53± 0.04	0.08± 0.03	116.70± 1.10	2599.0 ± 69.0	–	–	–	18.3	3.100	2093.070	–	12.3250	9,**12**,**61**,62,234
TIC 264770836	5078 ± 22	1.62± 0.14	5.44± 0.07	17.7± 0.29	−0.21± 0.02	11.26± 0.48	141.9 ± 3.3	–	–	–	129.4	1.510	623.000	–	2.5600	9,**101**,110
TIC 265052133	4788 ± 70	1.14± 0.05	2.62± 0.06	5.93± 0.02	0.39± 0.12	23.97± 0.46	353.3 ± 2.4	–	–	–	62.5	1.222	406.600	–	1.4900	9,110,131,**132**,141
TIC 268565917	6116 ± 110	1.21± 0.05	1.10	5.09± 0.05	0.27± 0.02	98.13± 0.14	2090.0 ± 20.0	–	–	–	29.9	0.500	119.600	–	1.0500	6,9,58,**60**
TIC 277774779	5909 ± 31	1.22± 0.06	–	2.34± 0.06	0.20± 0.10	81.02± 0.79	1547.4 ± 38.6	–	–	–	26.7	2.570	1359.000	–	4.2000	9,**23**,38,57
TIC 277890728	5847 ± 22	1.35± 0.01	1.95± 0.01	4.01± 0.01	0.33± 0.02	56.09± 0.19	1074.3 ± 20.7	–	–	–	31.1	10.150	10090.000	–	22.9000	9,38,**56**,103
TIC 284181945	4892 ± 23	2.66± 0.34	11.03± 0.65	**62.66**± 0.35	0.09 ±0.04	6.04± 0.13	73.5 ± 0.7	–	–	–	103.9	4.513	2142.000	–	4.3230	9,**17**,**22**,55
TIC 296740796	5901 ± 78	1.09± 0.04	1.39± 0.03	2.00± 0.07	0.04± 0.07	89.50	1900.0	–	–	–	11.9	0.124	15.508	–	0.0429	9,20,**21**,54
TIC 302372658	4698 ± 100	1.17± 0.20	7.47± 0.60	29.61± 0.27	−0.11± 0.10	5.64± 0.05	53.8 ± 2.0	–	–	–	183.1	1.149	415.400	–	3.9300	9,38,141,**230**
TIC 303193565	4947 ± 25	1.61± 0.04	4.67	17.66± 0.33	0.09± 0.01	12.41± 0.42	161.8 ± 7.5	–	–	–	192.2	1.262	428.500	–	2.7500	9,**14**,68,110,141
TIC 310836777	4661 ± 50	0.83± 0.07	10.22± 0.87	46.32± 0.21	−0.10± 0.06	3.86± 0.29	28.4 ± 3.5	–	–	–	121.7	0.594	157.350	–	2.8490	**17**,72,110,141
TIC 313709116	4760 ± 30	1.37± 0.05	4.80± 0.10	10.12± 0.04	0.18± 0.02	16.99± 0.28	237.2 ± 6.8	–	–	–	94.6	1.520	521.000	–	1.8000	9,**43**,110,141,210
TIC 325178933	4834 ± 59	1.38± 0.14	4.10± 0.60	9.45± 0.03	0.05± 0.10	15.60± 0.13	203.0 ± 3.6	–	–	–	91.7	1.830	871.190	–	1.5600	9,51,**52**
TIC 325254372	4760 ± 100	2.21± 0.57	6.30± 0.10	38.5± 0.72	0.12± 0.20	6.28± 0.55	74.3 ± 1.9	–	–	–	213.2	2.030	778.100	–	5.9000	9,**43**,110,119,141
TIC 332711151	4805 ± 100	0.89± 0.24	8.80± 0.60	51.47± 0.69	0.04± 0.10	5.52± 0.73	46.3 ± 3.9	–	–	–	213.8	2.720	1270.000	–	3.6000	9,**52**,53,110,141
TIC 334753043	4840	1.45± 0.09	4.85	12.73± 0.06	0.09	14.93± 0.17	194.9 ± 3.1	–	–	–	30.0	2.65	1285.00	–	1.8100	9,**14**,17,38,50
TIC 341687229	4883 ± 100	1.52± 0.11	11.21± 0.66	64.57± 9.4	−0.17± 0.10	4.34± 0.08	39.8 ± 1.7	–	–	–	108.9	1.080	310.400	–	0.9700	9,110,**117**,121
TIC 344627954	4871 ± 25	1.11± 0.05	4.06	9.67± 0.08	0.16± 0.01	16.58± 0.55	212.0 ± 5.4	–	–	–	121.3	1.570	637.100	–	1.5560	9,**14**,68,110,141

Table A1 – *continued*

Host	$T_{\rm eff}$(K)	M(M$_\odot$)	R (R$_\odot$)	L (L$_\odot$)	[M/H]	$\Delta\nu$ (μHz)	$\nu_{\rm max}$ (μHz)	$\delta\nu_{02}$ (μHz)	ν_0 (μHz)	ν_1 (μHz)	d (pc)	a (AU)	P (day)	$R_{\rm p}$ (R$_{\rm J}$)	$M_{\rm p}$ (M$_{\rm J}$)	Ref
TIC 345078350	4950 ± 100	1.46± 0.03	5.08	13.35± 0.23	0.06± 0.20	14.56± 0.21	194.5 ± 3.9	–	–	–	135.5	1.360	464.400	–	1.2600	9,**14**,110,119,141
TIC 353988778	4919	1.50	4.63± 0.43	10.55± 0.04	0.00± 0.02	17.50± 0.04	230.5 ± 1.0	–	–	–	49.7	1.220	417.670	–	1.3970	**17**,38,48
TIC 354489950	**5054±81**	2.32± 0.09	8.80± 0.61	**43.05**± 0.37	**-0.10±0.12**	8.57	110.5	–	–	–	76.2	2.476	982.850	–	9.2070	9,**17**,110,135,141
TIC 359558085	4769 ± 50	1.41± 0.09	12.73± 3.89	94.56± 2.43	−0.25± 0.06	3.04± 0.05	24.3 ± 0.9	–	–	–	531.4	5.700	4100.000	–	6.0000	9,72,110,**133**,141
TIC 362661163	5773	1.13± 0.02	1.38± 0.06	1.98± 0.01	0.28± 0.03	90.00	–	5.7 ± 0.4	–	–	15.6	1.535	646.485	–	1.6770	9,46,47,**231**
TIC 380908091	4912	1.56± 0.07	1.97	14.03± 0.18	0.10	13.23± 0.09	155.7 ± 9.4	–	–	–	133.2	2.010	1032.300	–	1.4870	9,**14**,34,38,110
TIC 380966347	4946 ± 50	1.33± 0.07	5.01	13.03± 0.11	0.02± 0.06	14.44± 0.50	185.5 ± 4.5	–	–	–	118.3	1.700	676.600	–	1.1210	9,**14**,72,110,141
TIC 394125166	5362 ± 18	1.05± 0.02	–	2.88± 0.01	−0.13± 0.01	51.17± 0.47	858.0 ± 13.2	–	–	–	29.2	5.935	5478.690	–	9.6200	9,**12**,38,44,103
TIC 397587084	6205 ± 20	1.07± 0.17	–	2.26± 0.01	0.22± 0.04	98.00± 13.00	2096.0 ± 338.0	–	–	–	17.6	43.500	–	–	4.0000	9,15,**16**,110
TIC 399334674	5101 ± 25	1.00± 0.02	4.41	13.8± 0.07	−0.19± 0.03	15.83± 1.10	188.6 ± 15.8	–	–	–	72.9	1.063	340.940	–	2.0960	9,**14**,49 110,141
TIC 405228516	4900 ± 100	1.48± 0.12	5.14	14.48± 0.21	−0.20± 0.13	14.08± 0.68	186.6 ± 6.4	–	–	–	134.2	1.157	356.210	–	1.9270	9,**14**, 110,134,141
TIC 423862056	4856 ± 35	1.64± 0.57	4.98± 0.20	12.26± 0.06	0.14± 0.05	15.53± 2.10	222.6 ± 13.4	–	–	–	66.8	1.063	358.270	–	1.1940	9,**17**,110,141,201
TIC 437246853	4925	1.41	4.60	8.28± 0.06	−0.02± 0.03	19.02± 0.13	269.9 ± 7.5	–	–	–	113.2	1.260	433.800	–	1.9640	9,**14**,38,68
TIC 441462736	5080 ± 90	1.21± 0.07	2.94± 0.06	5.09± 0.05	−0.08± 0.08	28.94± 0.15	430.0 ± 18.0	–	–	–	95.4	0.122	14.276	0.8360	0.1900	9,**13**
TIC 441797545	4805 ± 50	1.17± 0.04	10.95± 0.54	56.36± 6.01	−0.16± 0.06	4.33± 0.13	36.5 ± 0.9	–	–	–	107.5	0.850	279.300	–	0.5700	9,72,110,**117**
TIC 443578538	4861 ± 50	1.48± 0.10	7.30± 0.33	28.38± 0.2	−0.03± 0.06	8.53± 0.43	96.7 ± 3.8	–	–	–	83.9	1.207	360.080	–	2.0820	9,**17**,72,110,141
TIC 444865362	4951 ± 35	1.26± 0.16	4.94± 0.55	14.34± 0.09	−0.13± 0.05	13.28± 0.79	162.7 ± 5.2	–	–	–	54.9	2.028	919.860	–	1.8810	9,**17**, 110,141,201
TIC 449145115	4972 ± 25	1.52± 0.05	6.48	18.19± 0.29	−0.07± 0.01	9.79± 0.12	115.9 ± 2.5	–	–	–	186.3	1.180	380.200	–	1.5420	9,**14**,68,110,141
TIC 452910671	4818 ± 50	1.80± 0.01	10.90± 0.81	58.93± 0.48	0.00± 0.06	4.47± 0.16	44.2 ± 1.9	–	–	–	109.6	1.117	312.080	–	0.8960	9,**17**,72,110,141
TIC 456826468	4974 ± 100	1.61± 0.06	4.54± 0.49	13.2± 0.07	0.07± 0.20	15.09± 0.63	210.8 ± 8.2	–	–	–	54.2	1.079	355.500	–	1.5150	9,**17**, 110,119,141
TIC 456871289	6121 ± 85	1.44± 0.03	2.57± 0.12	10.02± 0.07	−0.25± 0.06	36.16± 0.24	702.4 ± 11.2	–	–	–	26.2	0.770	201.900	–	1.0600	9,38,40,**41**,220
TIC 456905162	5641	1.13	1.79	3.01± 0.01	0.17	60.34± 0.44	1127.6 ± 20.7	–	–	–	33.2	2.140	1075.690	–	6.383	9,**14**,38,111
KIC 3425851	6379 ± 85	1.19± 0.05	1.33± 0.03	–	0.01± 0.10	92.60± 1.50	2038.0 ± 60.0	–	–	–	255.6	–	110.378	0.2638	–	5,9,72,**78**
KIC 7199397	5896 ± 75	1.33± 0.02	2.51± 0.06	–	−0.17± 0.10	38.63± 0.68	643.0 ± 17.0	–	707.8	552.9	427.4	0.482	105.890	0.9327	–	5,9,**78**
KIC 7296438	5790 ± 75	1.15± 0.06	1.35± 0.19	–	0.30± 0.10	88.70± 0.10	1848.0 ± 16.0	5.3 ± 0.3	1983.2	1540.8	167.1	–	173.928	0.0830	–	9,86,**87**,204
KIC 8554498	5753 ± 75	1.20± 0.15	1.79± 0.13	–	0.05± 0.10	61.98± 0.96	1153.0 ± 76.0	–	1011.3	–	573.5	0.058	4.780	0.6370	–	5,9,**147**
KIC 9088780	4887 ± 54	1.40± 0.30	4.11± 0.30	29.45	−0.11± 0.03	7.36± 0.03	76.7 ± 0.5	–	–	–	2259.4	0.226	33.181	0.8350	–	9,72,**87**,136
KIC 9414417	6253 ± 75	1.34± 0.09	1.92± 0.04	–	−0.13± 0.10	60.05± 0.27	1115.0 ± 32.0	4.5± 1.1	–	1059.6	212.2	0.306	53.506	0.2306	–	5,6,9,**78**

Note. Ref. 1: G. R. Davies et al. (2016), 2: N. M. Batalha et al. (2013), 3: G. W. Marcy et al. (2014), 5: D. Huber et al. (2013a), 6: C. Kayhan et al. (2019), 7: J. Zhang et al. (2019), 8: W. J. Chaplin et al. (2014), 9: Gaia Collaboration et al. (2021), 10: R. D. Haywood et al. (2018), 11: T. D. Morton et al. (2016), 12: F. Feng et al. (2022), 13: D. Huber et al. (2019), 14: J. K. Luhn et al. (2019), 15: M. P. Di Mauro et al. (2022), 16: M. Kuzuhara et al. (2013), 17: H.-Y. Teng et al. (2023), 18: E. K. Baines, J. T. Armstrong & G. T. van Belle (2013), 19: R. A. Wittenmyer et al. (2011), 20: T. S. Metcalfe et al. (2023), 21: L. J. Rosenthal et al. (2021), 22: W.-X. Lin, S.-B. Qian & L.-Y. Zhu (2024a), 23: F. Philipot et al. (2023), 24: K. G. Stassun, K. A. Collins & B. S. Gaudi (2017), 25: J. Setiawan et al. (2005), 26: M. I. Jones et al. (2021), 27: N. Saunders et al. (2025), 28: B. C. Addison et al. (2021), 29: R. A. Wittenmyer et al. (2009), 30: W.-X. Lin et al. (2024b), 31: T. L. Campante et al. (2019), 32: M. I. Jones et al. (2014), 33: A. Niedzielski et al. (2016), 34: K. Ment et al. (2018), 35: D. Montes et al. (2018), 36: A. S. Bonomo et al. (2023), 37: L. M. Weiss et al. (2024), 38: E. Hatt et al. (2023), 39: F. Paletou et al. (2015), 40: S. Borgniet et al. (2014), 41: S. Borgniet et al. (2017), 42: A. Bonfanti et al. (2015) 43: J. A. Johnson et al. (2011b), 44: M. Marmier et al. (2013), 45: A. Bressan et al. (2012), 46: F. Bouchy et al. (2005), 47: G. F. Benedict et al. (2022), 48: B. Sato et al. (2008), 49: J. Maldonado & E. Villaver (2016), 50: S. G. Sousa et al. (2015), 51: C. Jiang et al. (2020), 52: R. A. Wittenmyer et al. (2017a), 53: R. A. Wittenmyer et al. (2016), 54: J. M. Brewer et al. (2017), 55: E. Jofré et al. (2015), 56: A. Venner, A. Vanderburg & L. A. Pearce (2021), 57: G.-Y. Xiao et al. (2023), 58: L. Gizon et al. (2013), 60: D. Naef et al. (2001), 61: C. X. Huang et al. (2018), 62: D. Huber et al. (2022), 63: Tautvaišienė et al. (2022), 64: B.-C. Lee et al. (2015), 65: M. J. Giguere et al. (2012), 66: V. Perdelwitz et al. (2024), 67: W. H. Ball et al. (2020), 68: J. M. Brewer et al. (2016), 69: R. P. Butler et al. (2006), 70: D. Fischer et al. (2009), 71: R. A. Wittenmyer et al. (2016), 72: C. Soubiran, N. Brouillet & L. Casamiquela (2022), 73: R. E. Chen et al. (2023), 74: J. A. Johnson et al. (2010), 75: M. B. Nielsen et al. (2020), 76: M. I. Jones et al. (2015), 77: S. R. Kane et al. (2015), 78: B. J. Fulton & E. A. Petigura (2018), 79: C. D. Dressing et al. (2015), 80: C. Beard et al. (2024), 81: S. G. Sousa et al. (2018), 82: S. M. Mills et al. (2019), 83: S. C. Dubber et al. (2019), 84: J.-W. Xie (2014), 85: T. L. Campante et al. (2015), 86: S. Deheuvels et al. (2016), 87: C. J. Burke et al. (2014), 88: V. Silva Aguirre et al. (2015), 89: H. Valizadegan et al. (2022), 90: A. Leleu et al. (2023), 91: T. Barclay et al. (2013), 92: V. M. Rajpaul et al. (2021), 93: V. Van Eylen et al. (2014), 94: J. Zhang et al. (2021), 95: A. Pál et al. (2008), 96: R. L. Gilliland et al. (2013), 97: J. A. Carter et al. (2012), 98: W. J. Chaplin et al. (2013), 99: N. M. Batalha et al. (2011), 100: A. S. Bonomo et al. (2025), 101: G. Ottoni et al. (2022), 102: R. Luque et al. (2019), 103: S. G. Sousa et al. (2008) 104: H. Harakawa et al. (2015), 105: B. Sato et al. (2013), 106: G. Jeong et al. (2018), 107: A. Niedzielski et al. (2015), 108: T. Appourchaux et al. (2012), 109: W. J. Borucki et al. (2010a), 110: J. Zhou et al. (2024), 111: N. C. Santos, G. Israelian & M. Mayor (2004), 112: H.-Y. Teng et al. (2023), 113: T. Arentoft et al. (2019), 114: J. A. Johnson et al. (2011a), 115: E. González-Álvarez et al. (2017), 116: T. Arentoft et al. (2019), 117: H.-Y. Teng et al. (2022a), 118: J. Meléndez et al. (2008), 119: L. Ghezzi, B. T. Montet & J. A. Johnson (2018), 120: B. Deka-Szymankiewicz et al. (2018), 121: Y. J. Liu et al. (2014), 122: H.-Y. Teng et al. (2022b), 123: R. E. Luck (2017), 124: M. I. Jones et al. (2016), 125: W. Kang, S.-G. Lee & K.-M. Kim (2011), 126: M. L. Hill et al. (2021), 127: T. Trifonov et al. (2022), 128: G. Jeong et al. (2022), 129: R. Forsberg et al. (2022), 130: M. Ortiz et al. (2016), 131: M. Rice & J. M. Brewer (2020), 132: S. Meschiari et al. (2011), 133: M. Adamów et al. (2018), 134: N. Vernekar et al. (2024), 135: E. K. Baines et al. (2009), 136: W.-X. Lin et al. (2025a), 137: S. K. Grunblatt et al. (2018), 138: P. Gajdoš, M. Vaňko & Š. Parimucha (2019), 139: T. A. Berger et al. (2018), 140: D. Huber et al. (2013b), 141: Gaia Collaboration et al. (2018), 142: C. Pezzotti et al. (2022), 143: S. Stock, S. Reffert & A. Quirrenbach (2018), 144: S. Hekker & J. Meléndez (2007), 145: S. O'Toole et al. (2009), 146: L. Delrez et al. (2021), 147: J. L. Coughlin et al. (2016), 148: M. H. Pinsonneault et al. (2018), 149: G. R. Davies et al. (2015), 150: M. N. Lund et al. (2017), 201: Abdurro'uf et al. (2022), 202: L. Wang et al. (2016), 203: A. Frasca et al. (2016), 204: N. Grieves et al. (2018), 205: J. F. Rowe et al. (2014), 206: J. M. Brewer & D. A. Fischer (2018), 209: M. Tsantaki et al. (2014), 210: Y.-S. Ting et al. (2019), 211: E. A. Petigura et al. (2017), 212: R. F. Wilson et al. (2022), 213: C. Charbonnel et al. (2020), 214: D. Mahdi et al. (2016), 215: M. G. Soto, M. I. Jones & J. S. Jenkins (2021), 216: C. Aguilera-Gómez, I. Ramírez & J. Chanamé (2018), 217: N. C. Santos et al. (2013), 220: G. Gonzalez, M. K. Carlson & R. W. Tobin (2010), 221: L.-y. Zhang et al. (2023), 223: C. Aguilera-Gómez, M. I. Jones & J. Chanamé (2023), 224: C. Chavero et al. (2019), 225: C. Soubiran et al. (2022), 226: M. Hon et al. (2023), 227: C. Jiang et al. (2023), 228: D. K. Feuillet et al. (2016), 229: H.-Y. Teng et al. (2022a), 230: R. A. Wittenmyer et al. (2017b), 231: K. Goździewski, A. J. Maciejewski & C. Migaszewski (2007), 232: S. E. Thompson et al. (2018), 233: X. Dumusque et al. (2014), 234: L. Ghezzi et al. (2010), 235: A. Weeks et al. (2025), 236: T. L. Campante et al. (2017), 237: E. Furlan et al. (2018).

Table A2. Basic physical properties of the interior models of the solar-like oscillating planet hosts and the revised mass and radius of the planets. The reference frequencies are shown, defined as $\nu_0 = \nu_{\mathrm{min0}}$ and $\nu_1 = \nu_{\mathrm{min1}}$.

Host	T_{eff} (K)	M $\mathrm{M}_\odot$	R $\mathrm{R}_\odot$	L $\mathrm{L}_\odot$	t_9 Gyr	Z_0	Y_0	α	Z_s	$\Delta\nu$ μHz	ν_{max} μHz	$\delta\nu_{02}$ μHz	ν_0 μHz	ν_1 μHz	R_{p} $\mathrm{R_J}$	M_{p} $\mathrm{M_J}$	Met.
KIC 3544595	5624	0.86± 0.03	0.91± 0.01	0.74	9.06±0.09	0.0111	0.2693	1.8213	0.0095±0.0002	145.8	3265.7	7.5	3273.7	2541.3	0.1302	0.0119	DZTref
KIC 3632418	6088	1.30± 0.15	1.86± 0.08	4.30	3.29±0.37	0.0163	0.2797	1.4599	0.0110±0.0041	61.0	1126.5	4.6	1402.4	1035.4	0.1435	0.0222	DZTref
KIC 4141376	6151	1.03± 0.04	1.04± 0.02	1.40	2.11±0.13	0.0088	0.2678	1.5980	0.0077±0.0008	128.6	2794.2	11.9	2992.0	2441.7	0.1996	0.0160	DZTL
KIC 4143755	5747	0.91± 0.12	1.42± 0.08	1.99	11.13±0.41	0.0082	0.2635	1.5652	0.0062±0.0011	77.2	1354.1	–	1722.9	1126.1	0.2217	–	DZTL
KIC 4349452	6209	1.10± 0.05	1.28± 0.02	2.20	5.39±0.14	0.0151	0.2779	2.2431	0.0130±0.0027	98.0	1961.4	6.1	2292.6	1715.4	0.2386	0.0259	DZTref
KIC 4914423	5904	1.17± 0.07	1.49± 0.04	2.42	4.99±0.18	0.0195	0.2861	1.7106	0.0168±0.0038	81.5	1604.4	5.3	1809.3	1391.0	0.3097	0.0356	DZTref
KIC 5094751	5897	1.02± 0.08	1.32± 0.05	1.89	7.94±0.25	0.0155	0.2781	1.8321	0.0127±0.0026	91.1	1770.6	5.7	1943.9	1492.6	0.2107	0.0140	DZT
KIC 5866724	6211	1.26± 0.05	1.42± 0.02	2.71	2.72±0.13	0.0237	0.2946	1.8311	0.0193±0.0033	89.9	1838.9	7.4	2084.9	1646.5	0.1273	0.0077	DZTref
KIC 6196457	5934	1.19± 0.17	1.72± 0.10	3.30	5.36±0.42	0.0229	0.2929	1.8311	0.0201±0.0044	66.5	1229.2	–	1437.9	1077.0	0.3165	0.1989	DZTref
KIC 6278762	5046	0.71± 0.03	0.74± 0.01	0.32	11.98± 0.13	0.0069	0.2614	1.3963	0.0057±0.0008	179.7	4276.9	10.5	–	3106.2	0.0354	–	DZT
KIC 6448890	4828	1.39± 0.04	4.36± 0.06	9.32	3.61±0.14	0.0212	0.2896	1.8445	0.0212±0.0065	17.4	253.8	–	256.3	–	0.5993	0.0736	DZT
KIC 6521045	5861	1.19± 0.05	1.56± 0.03	2.60	4.03±0.14	0.0193	0.2943	1.4527	0.0152±0.0029	76.3	1477.1	5.4	1683.7	1303.9	0.1239	0.0254	DZTref
KIC 7277317	4812	1.06± 0.04	2.62± 0.06	3.32	9.11±0.15	0.0186	0.2843	1.7820	0.0182±0.0016	33.0	529.7	–	–	–	1.1103	0.9309	DZTR
KIC 7670943	6193	1.17± 0.06	1.41± 0.03	2.63	3.88±0.15	0.0150	0.2771	1.8311	0.0118±0.0003	87.9	1718.9	6.6	1957.1	1531.3	0.1479	–	DZT
KIC 8077137	6056	1.14± 0.11	1.64± 0.07	3.27	5.13±0.30	0.0145	0.2761	1.6301	0.0111±0.0016	69.5	1249.3	–	1541.1	1139.6	0.1254	0.0115	DZTref
KIC 8292840	6300	1.15± 0.04	1.34± 0.02	2.54	3.56±0.11	0.0129	0.2729	1.8311	0.0095±0.0014	93.7	1835.3	7.5	2080.2	1671.5	0.1299	–	DZTref
KIC 8349582	5648	1.09± 0.07	1.43± 0.04	1.89	6.77±0.21	0.0261	0.2994	1.5418	0.0216±0.0048	83.6	1664.6	5.3	1770.1	1370.4	0.3101	0.0415	DZTL
KIC 8478994	5370	0.76± 0.03	0.76± 0.01	0.43	9.20±0.12	0.0075	0.2621	1.8311	0.0064±0.0013	178.8	4147.2	10.7	–	3422.7	0.0266	–	DZTR
KIC 8494142	6179	1.38± 0.30	1.88± 0.14	4.65	2.94±0.66	0.0200	0.2871	1.8311	0.0166±0.0037	62.0	1143.4	4.5	1370.6	1058.6	0.2399	0.1217	DZTref
KIC 8866102	6372	1.25± 0.05	1.38± 0.02	2.85	2.29±0.12	0.0205	0.2955	1.9311	0.0163±0.0034	93.0	1889.7	7.9	2062.0	–	0.2584	–	MinZ
KIC 9592705	6143	1.47± 0.10	2.12± 0.06	5.79	2.54±0.22	0.0253	0.2977	1.6511	0.0200±0.0046	53.3	958.2	4.0	–	915.4	0.2966	–	DZTR
KIC 9955598	5378	0.86± 0.04	0.88± 0.01	0.58	9.04±0.15	0.0169	0.2809	1.8311	0.0148±0.0030	152.9	3550.1	8.6	–	2715.9	0.1048	0.0179	DZTref
KIC 10585852	4992	1.00± 0.04	3.19± 0.07	5.71	10.06±0.13	0.0136	0.2743	2.1004	0.0134±0.0009	23.5	332.2	–	335.5	–	0.3428	–	DZT
KIC 10586004	5793	1.19± 0.14	1.67± 0.09	2.84	6.33±0.36	0.0271	0.2852	1.8311	0.0240±0.0050	69.4	1316.7	–	1417.6	1124.1	0.2164	0.0061	DZTref
KIC 10593626	5715	0.84± 0.03	0.93± 0.01	0.84	11.25±0.11	0.0089	0.2649	1.8311	0.0072±0.0012	137.6	2913.2	6.0	–	–	0.2011	0.0283	DZT
KIC 10666592	6418	1.57± 0.22	2.01± 0.10	6.19	1.56±0.43	0.0314	0.3099	1.8243	0.0189±0.0037	59.1	1082.8	4.7	1235.8	1117.7	1.4875	1.9045	DZTL
KIC 10963065	6169	1.07± 0.04	1.22± 0.02	1.94	4.51±0.13	0.0120	0.2712	1.7811	0.0096±0.0020	103.9	2096.4	7.3	2341.7	1820.2	0.0726	0.0016	DZTref
KIC 11295426	5755	1.00± 0.03	1.22± 0.01	1.47	8.52±0.09	0.0196	0.2864	1.8250	0.0166±0.0026	101.6	2083.1	5.4	–	1720.8	0.2036	0.0240	DZTref
KIC 11401755	5927	1.11± 0.14	1.65± 0.09	3.01	5.24±0.38	0.0110	0.2691	1.2018	0.0054±0.0013	67.9	1174.5	–	1358.4	1085.2	0.1342	0.0141	DZTref
KIC 11673802	4924	1.07± 0.08	3.47± 0.13	6.39	8.69±0.22	0.0171	0.2814	2.0502	0.0169±0.0012	21.3	303.0	–	304.4	–	0.5739	–	DZTR
KIC 11807274	6184	1.21± 0.05	1.57± 0.02	3.25	3.36±0.14	0.0132	0.2783	1.5711	0.0086±0.0014	75.8	1402.6	5.9	1596.3	1292.1	0.1521	–	DZTL
KIC 11853905	5825	1.12± 0.12	1.56± 0.08	2.54	6.75±0.33	0.0231	0.2932	1.8311	0.0201±0.0026	74.3	1408.8	4.8	1503.9	1208.1	0.3748	0.0706	DZTL
KIC 11904151	5762	0.91± 0.09	1.06± 0.03	1.12	10.07±0.30	0.0128	0.2727	1.8345	0.0106±0.0009	118.2	2450.3	5.6	–	2023.1	0.1303	0.0102	DZTL
KIC 12069449	5750	0.97± 0.02	1.10± 0.01	1.18	8.12±0.08	0.0177	0.2825	1.8311	0.0151±0.0007	117.1	2490.4	6.1	2613.3	2003.4	–	1.7341	DZTref
TIC 612908	4967	1.12± 0.22	4.85± 0.45	12.90	6.34±0.59	0.0097	0.2665	1.9926	0.0097±0.0004	13.2	160.6	–	166.9	–	1.3534	1.4765	DZTL
TIC 1713457	4990	1.08± 0.11	4.59± 0.17	11.75	7.50±0.30	0.0109	0.2689	2.0874	0.0108±0.0005	14.1	173.0	–	180.3	–	–	1.3897	DZT
TIC 12723961	4996	1.52± 0.20	4.72± 0.22	12.49	2.12±0.40	0.0122	0.2776	1.8311	0.0122±0.0025	16.2	231.8	–	239.0	–	–	2.3351	DZTR
TIC 13105061	4298	1.14± 0.22	11.20± 0.86	38.57	6.35±0.58	0.0114	0.2699	1.4936	0.0114±0.0035	3.8	32.7	–	–	–	–	12.6393	DZT
TIC 17554529	4957	2.39± 0.4	11.88± 0.7	76.86	0.80± 0.05	0.0189	0.2849	1.8311	0.0191±0.0009	5.0	56.4.1	–	66.1	–	–	6.8937	DZLTe3
TIC 20537900	4934	1.00± 0.14	4.51± 0.30	10.88	9.63±0.44	0.0102	0.2674	2.0243	0.0101±0.0011	13.9	166.6	–	168.5	–	–	1.4609	DZT
TIC 28763463	4889	1.68± 0.3	11.24± 1.04	65.02	1.43± 0.55	0.0097	0.2665	1.8767	0.0098±0.0004	4.8	33.4	–	51.9	40.4	–	0.5374	DZLTe3
TIC 38828538	4787	1.28± 0.04	4.71± 0.06	10.48	4.66±0.11	0.0186	0.2842	1.8311	0.0185±0.0038	14.9	201.9	–	206.3	–	–	1.7218	DZT
TIC 46310554	4866	1.23± 0.06	3.36± 0.09	5.70	5.75±0.21	0.0250	0.2970	1.9558	0.0248±0.0027	24.2	379.1	–	375.7	–	–	0.9749	DZTL
TIC 48237215	4795	1.50± 0.05	5.24± 0.06	13.09	2.76±0.11	0.0217	0.2904	1.8311	0.0217±0.0045	13.7	191.2	–	194.3	–	–	2.0234	DZTL
TIC 49430557	4780	1.79± 0.62	11.64± 2.11	63.72	1.37± 1.11	0.0111	0.2693	1.7756	0.0112±0.0007	4.6	43.2	–	50.1	38.9	–	0.5944	DZLTe3

Table A2 – *continued*

Host	$T_{\rm eff}$ (K)	M $M_\odot$	R $R_\odot$	L $L_\odot$	t_9 Gyr	Z_0	Y_0	α	Z_s	$\Delta\nu$ μHz	$\nu_{\rm max}$ μHz	$\delta\nu_{02}$ μHz	ν_0 μHz	ν_1 μHz	$R_{\rm p}$ $R_{\rm J}$	$M_{\rm p}$ $M_{\rm J}$	Met.
TIC 53178442	5015	1.04± 0.31	3.78± 0.56	8.14	8.11±0.90	0.0095	0.2661	2.0058	0.0094±0.0012	18.5	244.0	–	246.8	–	–	0.9627	DZT
TIC 53873088	4928	1.62± 0.08	5.77± 0.14	17.66	2.04±0.15	0.0184	0.2839	1.9736	0.0185±0.0016	12.3	167.3	–	173.4	–	–	1.3286	DZTR
TIC 57983992	4902	1.56± 0.18	4.07± 0.16	8.62	2.33±0.34	0.0222	0.2915	1.8311	0.0222±0.0024	20.6	325.9	–	–	–	–	1.0985	DZTL
TIC 63905972	4946	1.53± 0.26	5.07± 0.29	13.89	2.21±0.52	0.0130	0.2732	1.8311	0.0131±0.0012	14.5	202.2	–	207.8	–	–	2.1898	DZTL
TIC 68418284	4961	1.71± 0.25	8.78± 0.49	42.06	1.69±0.45	0.0174	0.2819	2.2630	0.0175±0.0012	6.6	76.1	–	81.8	–	–	4.0453	DZT
TIC 71099944	4882	1.78± 0.22	9.27± 0.45	44.01	1.23±0.38	0.0085	0.2640	1.8311	0.0085±0.0017	6.3	70.5	–	75.7	–	–	2.4053	DZT
TIC 71345433	4942	1.21± 0.19	5.87± 0.36	18.55	5.00±0.48	0.0117	0.2704	2.0715	0.0117±0.0015	10.2	119.7	–	124.0	–	–	3.0308	DZT
TIC 77481104	4793	1.21± 0.40	6.75± 1.08	21.69	5.58±1.00	0.0161	0.2793	2.0420	0.0161±0.0011	8.3	92.2	–	–	–	–	1.4780	DZT
TIC 82604982	4671	1.34± 0.31	11.33± 1.26	55.02	3.22±0.70	0.0081	0.2632	1.8311	0.0081±0.0014	4.0	36.3	–	–	–	–	1.3140	DZTL
TIC 95361265	4808	1.06± 0.36	10.70± 1.65	55.11	7.35±1.02	0.0085	0.2640	2.2192	0.0084±0.0014	3.9	31.9	–	–	–	–	2.3066	DZTR
TIC 95473936	5498	1.03± 0.09	1.90± 0.07	2.96	8.29±0.25	0.0117	0.2706	1.8311	0.0109±0.0007	53.6	908.1	–	–	734.6	–	7.0198	DZTL
TIC 111947706	4820	1.20± 0.10	5.53± 0.17	14.88	5.15±0.26	0.0114	0.2699	1.8311	0.0114±0.0023	11.2	135.0	–	138.6	–	–	0.9902	DZTL
TIC 113329742	5015	1.13± 0.11	5.04± 0.20	14.49	6.11±0.31	0.0097	0.2665	2.0875	0.0097±0.0020	12.4	149.6	–	155.1	–	–	0.2592	DZT
TIC 117905020	5258	0.98± 0.10	2.36± 0.13	3.83	8.63±0.38	0.0070	0.2612	2.0527	0.0068±0.0000	37.2	571.3	–	–	456.0	–	4.9125	DZT
TIC 122555698	5778	1.08± 0.13	1.61± 0.08	2.62	8.00±0.36	0.0197	0.2864	1.9839	0.0175±0.0028	69.5	1278.3	–	1344.2	1081.8	–	0.0625	DZTL
TIC 129649472	4670	1.04± 0.15	10.68± 0.74	48.83	6.96± 0.43	0.0196	0.2863	2.0165	0.0197±0.0030	4.1	31.2	–	39.1	27.1	–	4.0447	DZLTe3
TIC 136916387	5665	0.86± 0.04	1.02±0.02	0.97	11.51± 0.14	0.0097	0.2664	1.6237	0.0077±0.0008	122.1	2563.0	5.7	–	2060.6	0.1433	0.0147	DZTR
TIC 137810576	4981	1.74± 0.16	4.63± 0.16	11.88	1.65±0.28	0.0238	0.2947	1.9449	0.0239±0.0014	17.8	269.9	–	287.1	–	–	0.9927	DZTL
TIC 138764379	4797	1.27± 0.08	4.67± 0.11	10.43	4.76±0.20	0.0177	0.2825	1.8311	0.0177±0.0037	15.0	196.9	–	205.9	–	–	1.4413	DZTL
TIC 146264536	4841	1.43± 0.28	7.52± 0.68	28.02	3.04±0.58	0.0149	0.2770	2.0269	0.0150±0.0010	7.7	85.0	–	92.2	–	–	2.4178	DZTL
TIC 148153804	4846	1.12± 0.08	4.54± 0.12	10.25	7.95±0.21	0.0228	0.2926	2.1125	0.0227±0.0015	14.6	183.7	–	191.7	–	–	1.5495	DZTL
TIC 148680230	4897	1.22± 0.29	5.76± 0.63	17.21	5.14±0.72	0.0140	0.2752	2.0509	0.0140±0.0009	10.6	123.2	–	130.0	–	–	1.0270	DZT
TIC 156942082	4857	1.18± 0.25	7.84± 0.86	30.83	5.88±0.78	0.0150	0.2772	2.2518	0.0150±0.0010	6.5	64.8	–	–	–	–	0.8350	DZT
TIC 160224839	4702	0.81± 0.13	11.79± 0.97	61.21	9.86± 0.48	0.0072	0.2615	1.6984	0.0072±0.0008	3.1	20.1	–	–	20.8	–	3.7083	DZLTe3
TIC 165722603	4504	1.34± 0.07	11.37± 0.21	47.96	3.78±0.16	0.0144	0.2758	1.7888	0.0144±0.0024	4.0	36.3	–	–	–	–	10.2934	DZT
TIC 169397663	5049	1.10± 0.07	3.82± 0.09	8.53	7.50±0.20	0.0144	0.2758	2.2110	0.0143±0.0010	18.8	248.5	–	260.8	–	–	0.9080	DZT
TIC 169534187	4859	1.59± 0.09	5.61± 0.14	15.81	2.30±0.18	0.0248	0.2967	1.9716	0.0249±0.0047	12.7	170.2	–	182.0	–	–	1.8675	DZTL
TIC 176379354	5868	1.14± 0.03	1.56± 0.01	2.61	6.23±0.09	0.0242	0.2955	1.8311	0.0212±0.0020	74.9	1426.8	5.3	1526.3	1241.6	–	1.2039	DZT
TIC 198079199	4780	1.49± 0.19	3.92± 0.17	7.24	3.12±0.38	0.0287	0.2944	1.7811	0.0287±0.0043	21.2	328.6	–	–	–	–	1.8896	DZTL
TIC 200093173	5578	1.52± 0.29	2.74± 0.24	6.53	2.82±0.57	0.0294	0.2940	1.8311	0.0281±0.0036	37.7	637.3	–	739.9	552.1	–	1.0060	DZTL
TIC 200723869	6161	1.33± 0.19	1.88± 0.12	4.57	3.62±0.43	0.0310	0.3121	2.0311	0.0282±0.0058	61.7	1133.1	–	1431.1	1047.0	0.6408	0.1304	DZTR
TIC 201175570	4701	1.14± 0.06	4.23± 0.08	7.87	7.59±0.16	0.0240	0.2951	1.8311	0.0238±0.0049	16.5	218.5	–	227.2	–	1.0521	0.3839	DZT
TIC 224312054	4597	1.39± 0.18	11.17± 0.57	50.21	3.76±0.39	0.0208	0.2886	2.0640	0.0209±0.0023	4.2	38.5	–	–	–	–	10.2480	DZT
TIC 225884682	4896	1.37± 0.10	4.93± 0.12	12.58	3.27±0.22	0.0131	0.2733	1.8311	0.0131±0.0014	14.4	189.7	–	200.7	–	–	1.9200	DZT
TIC 231019255	4654	1.03± 0.11	7.15± 0.35	21.63	8.77±0.31	0.0106	0.2684	1.8055	0.0105±0.0009	7.0	69.4	–	–	–	–	4.5947	DZTL
TIC 232074535	4973	1.90± 0.09	11.32± 0.25	70.59	1.01± 0.15	0.0082	0.2635	1.8311	0.0083±0.0017	5.0	49.4	–	59.3	44.2	–	6.5098	DZLTe3
TIC 232620788	5503	1.11± 0.18	1.82± 0.15	2.74	7.83±0.49	0.0235	0.2942	1.8311	0.0216±0.0045	59.1	1056.2	–	–	868.2	–	0.7737	DZTL
TIC 233008631	4205	0.99± 0.33	17.94± 0.13	90.77	10.48±1.46	0.0114	0.2699	1.7543	0.0113±0.0000	1.8	11.1	–	–	–	–	1.8277	DZTL
TIC 236339228	4745	1.02± 0.21	9.81± 0.87	43.96	8.51±0.76	0.0083	0.2636	2.0734	0.0082±0.0009	4.3	36.5	–	–	–	–	1.5500	DZT
TIC 246937460	4858	1.07± 0.33	10.70± 1.65	57.45	5.20± 0.93	0.0095	0.2661	1.9817	0.0096±0.0012	4.1	31.6	–	42.5	27.6	–	6.6672	DZLTe3
TIC 247119634	4671	1.75± 0.61	12.67± 2.22	68.92	1.47± 1.05	0.0163	0.2797	1.8011	0.0165±0.0007	4.0	37.4	–	43.6	–	–	6.3750	DZLTe3
TIC 257005016	4836	1.56± 0.08	10.91± 0.23	58.70	1.79± 0.16	0.0125	0.2721	1.9131	0.0126±0.0026	4.8	44.1	–	–	–	–	1.7005	DZLTeC
TIC 261136679	5985	1.05± 0.04	1.13± 0.02	1.47	4.93±0.10	0.0179	0.2829	1.9049	0.0157±0.0011	116.6	2508.0	7.9	2717.3	2095.9	–	11.7902	DZTL
TIC 264770836	5081	1.31± 0.23	5.68± 0.49	19.40	3.43±0.54	0.0082	0.2635	2.0622	0.0082±0.0004	11.2	135.1	–	145.0	–	–	2.0395	DZTR
TIC 265052133	4778	1.25± 0.08	3.41± 0.12	5.46	5.70±0.26	0.0329	0.3129	1.8882	0.0327±0.0079	23.9	380.6	–	375.1	–	–	1.2621	DZT

Table A2 – *continued*

Host	$T_{\rm eff}$ (K)	M $M_\odot$	R $R_\odot$	L $L_\odot$	t_9 Gyr	Z_0	Y_0	α	Z_s	$\Delta\nu$ μHz	$\nu_{\rm max}$ μHz	$\delta\nu_{02}$ μHz	ν_0 μHz	ν_1 μHz	$R_{\rm p}$ $R_{\rm J}$	$M_{\rm p}$ $M_{\rm J}$	Met.
TIC 268565917	6015	1.17± 0.03	1.31± 0.01	2.04	3.81±0.08	0.0250	0.2971	1.8311	0.0217±0.0009	97.9	2061.8	6.9	2283.6	1784.5	–	1.0448	DZTR
TIC 277774779	5913	1.13± 0.05	1.48± 0.03	2.42	5.97±0.13	0.0241	0.2954	1.8311	0.0213±0.0044	81.0	1580.5	5.6	1717.0	1348.6	–	3.9016	DZTL
TIC 277890728	5850	1.26± 0.08	1.97± 0.05	4.09	4.75±0.18	0.0319	0.3173	2.0761	0.0295±0.0013	55.9	1023.2	–	1168.8	872.7	–	21.3966	DZTL
TIC 284181945	4894	2.19± 0.18	10.33± 0.44	55.18	0.76± 0.25	0.0164	0.2799	1.8895	0.0166±0.0034	6.0	68.7	–	78.9	–	–	3.5512	DZLTeC
TIC 296740796	5920	1.06± 0.04	1.35± 0.02	2.01	7.00±0.12	0.0176	0.2823	1.8311	0.0146±0.0022	90.0	1759.9	5.6	1913.1	1479.1	–	0.0432	DZTL
TIC 302372658	4645	1.14± 0.14	8.60± 0.36	31.03	6.14±0.36	0.0105	0.2682	1.8311	0.0105±0.0021	5.6	54.0	–	–	–	–	3.8290	DZTL
TIC 303193565	4952	1.25± 0.23	5.25± 0.42	14.94	4.98±0.57	0.0165	0.2801	2.1444	0.0165±0.0004	12.3	155.0	–	162.0	–	–	2.3480	DZT
TIC 310836777	4658	0.98± 0.33	10.35± 0.16	45.44	10.57±1.39	0.0106	0.2684	2.0908	0.0105±0.0014	3.9	32.0	–	–	–	–	2.4708	DZTL
TIC 313709116	4890	1.40± 0.11	4.45± 0.17	10.18	3.45±0.32	0.0201	0.2873	1.9266	0.0201±0.0009	16.9	245.4	–	248.9	–	–	1.5310	DZTL
TIC 325178933	4883	1.37± 0.09	4.64± 0.12	11.03	3.38±0.21	0.0150	0.2771	1.8311	0.0150±0.0033	15.7	218.9	–	222.4	–	–	2.0024	DZT
TIC 325254372	4758	1.77± 0.62	9.23± 1.60	39.39	1.51±1.05	0.0177	0.2824	1.9286	0.0178±0.0065	6.3	72.6	–	77.6	–	–	5.3618	DZTL
TIC 332711151	4754	1.02± 0.43	8.36± 0.28	32.14	9.93±1.71	0.0147	0.2765	2.2311	0.0145±0.0030	5.5	51.0	–	–	–	–	2.2311	DZT
TIC 334753043	4842	1.36± 0.09	4.79± 0.14	11.39	3.64±0.21	0.0165	0.2801	1.8311	0.0165±0.0034	14.9	204.1	–	210.2	–	–	1.6389	DZTR
TIC 341687229	4888	1.23± 0.18	10.47± 0.59	56.44	4.43±0.45	0.0091	0.2652	2.2722	0.0091±0.0019	4.3	38.4	–	–	–	–	0.6795	DZT
TIC 344627954	4871	1.11± 0.14	4.15± 0.27	8.74	8.10±0.45	0.0194	0.2858	2.0618	0.0193±0.0004	16.6	222.5	–	224.2	–	–	1.3550	DZT
TIC 345078350	4951	1.15± 0.10	4.59± 0.17	11.39	6.57±0.28	0.0154	0.2779	2.1115	0.0153±0.0057	14.5	186.2	–	190.9	–	–	0.9372	DZT
TIC 353988778	4866	1.16± 0.04	4.09± 0.05	8.45	5.92±0.09	0.0132	0.2735	1.8311	0.0131±0.0006	17.5	238.1	–	242.6	–	–	1.1680	DZT
TIC 354489950	5063	2.39± 0.11	8.43± 0.20	42.03	0.57± 0.15	0.0117	0.2705	1.8311	0.0118±0.0024	8.5	110.9	–	124.8	–	–	10.4789	DZLTe3
TIC 359558085	4770	1.15± 0.15	12.86± 0.62	77.15	5.33±0.38	0.0075	0.2622	2.1779	0.0075±0.0010	3.0	23.9	–	–	–	–	4.6868	DZT
TIC 362661163	5728	1.15± 0.04	1.39± 0.02	1.88	5.61±0.10	0.0300	0.3071	1.8311	0.0271±0.0017	89.3	1879.7	4.9	1989.7	1534.6	–	1.8767	DZTL
TIC 380908091	4852	1.49± 0.27	5.36± 0.32	14.34	2.63±0.54	0.0164	0.2800	1.8311	0.0165±0.0035	13.2	179.1	–	186.0	–	–	2.1926	DZTL
TIC 380966347	4943	1.03± 0.16	4.45± 0.32	10.66	9.32±0.46	0.0140	0.2752	2.1399	0.0139±0.0018	14.4	177.7	–	183.1	–	–	0.8082	DZT
TIC 394125166	5361	1.01± 0.06	1.94± 0.06	2.80	8.93±0.19	0.0107	0.2685	1.8311	0.0101±0.0002	51.1	860.3	–	–	691.6	–	10.5559	DZTL
TIC 397587084	6220	1.25± 0.34	1.34± 0.22	2.42	2.20±0.83	0.0260	0.2991	1.8311	0.0220±0.0134	98.0	2075.8	8.5	2272.3	1853.0	–	4.1023	DZT
TIC 399334674	5100	1.00± 0.29	4.16± 0.61	10.55	8.89±1.09	0.0087	0.2644	2.1928	0.0086±0.0006	15.8	193.1	–	–	–	–	1.5241	DZT
TIC 405228516	4891	1.12± 0.24	4.68± 0.47	11.28	5.87±0.65	0.0085	0.2640	1.7832	0.0085±0.0022	14.0	174.6	–	–	–	–	1.3291	DZT
TIC 423862056	4855	1.28± 0.71	4.56± 1.24	10.43	4.71±1.66	0.0185	0.2842	1.9273	0.0185±0.0020	15.6	212.5	–	–	–	–	1.2208	DZT
TIC 437246853	4924	1.21± 0.10	3.91± 0.12	8.11	5.51±0.26	0.0166	0.2803	1.9700	0.0165±0.0010	19.0	270.6	–	271.8	–	–	1.6831	DZTL
TIC 441462736	5046	1.23± 0.16	2.99± 0.13	5.23	4.54±0.39	0.0113	0.2697	1.8311	0.0111±0.0019	28.9	455.9	–	459.4	–	0.8510	0.1926	DZTL
TIC 441797545	4803	1.31± 0.16	11.11± 0.66	59.22	2.92± 0.37	0.0093	0.2657	1.8418	0.0094±0.0012	4.3	36.0	–	41.7	33.1	–	0.7064	DZLTe3
TIC 443578538	4860	1.17± 0.26	6.58± 0.70	21.76	5.84±0.68	0.0125	0.2721	2.0622	0.0125±0.0016	8.5	92.8	–	–	–	–	1.3428	DZT
TIC 444865362	4953	0.98± 0.25	4.61± 0.56	11.53	10.19±0.75	0.0100	0.2671	2.0762	0.0099±0.0011	13.2	156.4	–	161.3	–	–	1.3997	DZT
TIC 449145115	4998	1.21± 0.10	6.05± 0.19	20.59	5.01±0.24	0.0114	0.2699	2.1819	0.0114±0.0003	9.8	112.0	–	118.2	–	–	1.2192	DZT
TIC 452910671	4818	1.50± 0.28	10.91± 0.89	57.76	2.52±0.56	0.0134	0.2739	2.1837	0.0135±0.0017	4.5	43.5	–	–	–	–	0.7022	DZTL
TIC 456826468	4980	1.28± 0.26	4.64± 0.42	11.94	4.49±0.61	0.0157	0.2786	2.0764	0.0157±0.0058	15.0	201.8	–	208.2	–	–	1.4526	DZT
TIC 456871289	6128	1.32± 0.08	2.67± 0.06	9.03	2.62±0.18	0.0094	0.2934	1.7811	0.0071±0.0010	36.0	542.9	–	–	536.7	–	0.9347	DZT
TIC 456905162	5680	1.14± 0.07	1.81± 0.05	3.08	6.63±0.19	0.0206	0.2883	1.6776	0.0180±0.0012	60.4	1080.7	–	1183.0	908.5	–	6.4277	DZTL
KIC 3425851	6371	1.26± 0.06	1.40± 0.03	2.90	2.30±0.16	0.0188	0.2846	1.8311	0.0139±0.0028	91.6	1838.4	8.0	2306.0	1736.3	0.2773	–	DZT
KIC 7199397	5887	1.35± 0.14	2.57± 0.12	7.17	3.14±0.32	0.0117	0.2705	1.8827	0.0108±0.0019	38.6	616.6	–	724.3	549.7	0.9566	–	DZTref
KIC 7296438	5835	1.09± 0.04	1.37± 0.02	1.97	6.95±0.12	0.0273	0.3071	1.9421	0.0237±0.0046	88.7	1791.4	5.3	1980.9	1496.3	0.0844	–	DZTref
KIC 8554498	5915	1.20± 0.24	1.81± 0.13	3.61	5.15±0.61	0.0207	0.2886	1.7381	0.0177±0.0039	61.9	1117.4	–	1290.6	972.0	0.6434	–	DZTR
KIC 9088780	4894	1.08± 0.04	7.03± 0.09	25.58	7.25±0.11	0.0104	0.2679	2.1564	0.0103±0.0007	7.3	74.9	–	–	–	1.4290	–	DZT
KIC 9414417	6212	1.33± 0.12	1.88± 0.07	4.74	3.15±0.27	0.0164	0.2774	1.6033	0.0118±0.0022	60.8	1081.0	4.6	1276.3	1031.8	0.2256	–	DZTref

APPENDIX B: PLANET HOSTS WITH VERY LOW METALLICITIES

Two planet hostswith very low metallicities reported in the literature are TOI-2018 and HD 155358, with [M/H] values of −0.58 dex (F. Dai et al. 2023) and −0.60 dex (K. G. Stassun et al. 2017), respectively. No asteroseismic constraints are currently available for these stars. Their observed [α/Fe] values, 0.29 (F. Dai et al. 2023) and 0.10 (A. E. García Pérez et al. 2021), imply surface heavy-element abundances of $Z_s = 0.006$ and $Z_s = 0.004$, respectively. These values are lower than the critical initial metallicity obtained for the planet-host sample ($Z_0 \simeq 0.007$). To investigate whether these systems indeed formed with lower initial metallicities, stellar interior models including microscopic diffusion were constructed.

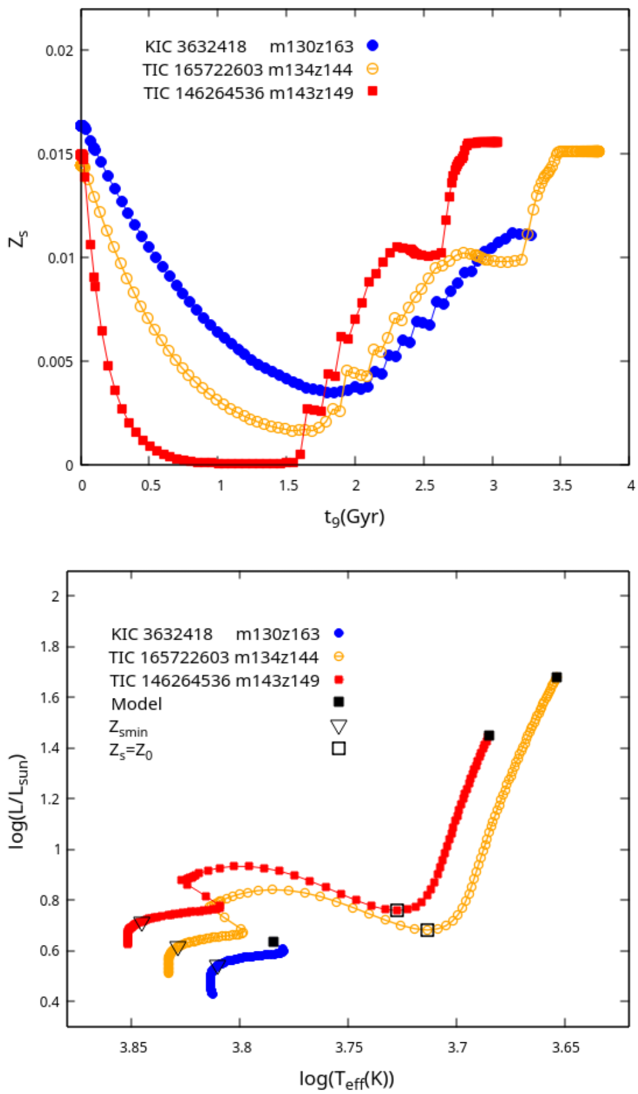

Figure B1. (a) Temporal evolution of Z_s for three planet hosts: KIC 3632418 (filled circles), TIC 165722603 (open circles), and TIC 146264536 (filled squares). For the latter two stars, the present-day Z_s remains close to Z_0 because these evolved objects experience the first dredge-up, which restores heavy elements previously depleted by diffusion. (b) Corresponding evolutionary tracks in the HR diagram. Filled symbols indicate the present-day positions of the stars, while triangles mark the evolutionary phase where Z_s reaches its minimum value. The box corresponds to the $Z_s = Z_0$ case.

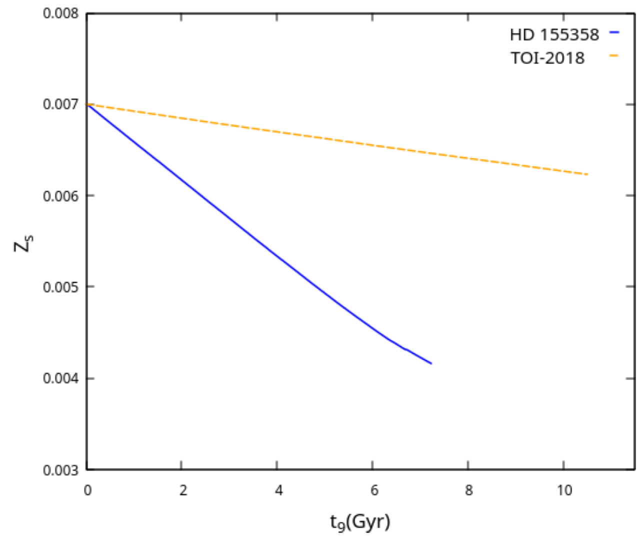

Figure B2. Evolution of the surface heavy-element abundance Z_s as a function of stellar age t_9 for TOI-2018 (dashed line) and HD 155358 (solid line). Both models adopt an initial heavy-element abundance $Z_0 = 0.007$. Due to microscopic diffusion, Z_s decreases to present-day values of 0.006 and 0.004, respectively.

Among the 127 planet hosts analysed in this study, several stars exhibit present-day surface metallicities around $Z_s \sim 0.004$–0.005 despite having initial abundances $Z_0 > 0.007$. Three representative examples – KIC 3632418, TIC 165722603, and TIC 146264536 – experienced phases during their evolution in which Z_s became very low. Fig. B1 shows the evolution of Z_s with age for these stars, all having $Z_0 \simeq 0.015$. The decrease in Z_s depends strongly on stellar mass. For KIC 3632418 (1.30 $M_\odot$), Z_s decreases to ~ 0.004 at $t_9 \approx 2$ Gyr; for TIC 165722603 (1.34 $M_\odot$), it reaches ~ 0.002 at $t_9 \approx 1.5$ Gyr; and for TIC 146264536 (1.43 $M_\odot$), Z_s becomes nearly zero between $t_9 = 0.5$–1.5 Gyr. These examples demonstrate that very low surface metallicities can naturally arise during stellar evolution even for relatively metal-rich initial compositions. This behaviour is also reflected in the evolutionary tracks shown in Fig. B1(b), where the minimum values of Z_s occur during the MS phase. As the stars evolve toward the RGB, the deepening convective envelope restores the surface composition, driving Z_s back toward its initial value Z_0.

The model properties of TOI-2018 and HD 155358 are listed in Table B1, and the evolution of Z_s is shown in Fig. B2. Both stars are reproduced with an initial heavy-element abundance $Z_0 = 0.007$. The model age of TOI-2018 is 10.5 Gyr, while HD 155358 has an age of 7.23 Gyr. Owing to its low mass (0.57 $M_\odot$), diffusion operates slowly in TOI-2018, resulting in a small difference between Z_0 and Z_s (~ 0.001). In contrast, diffusion is more efficient in HD 155358, producing a larger difference of ~ 0.003. The evolutionary models of both stars are fully consistent with the results presented in Section 4.6. These results demonstrate that very low present-day surface metallicities do not necessarily imply low initial heavy-element abundances, and that stellar evolution effects, particularly microscopic diffusion, naturally reconcile the observed properties of these systems with a common initial metallicity threshold of $Z_0 \simeq 0.007$ for planet-host stars.

Table B1. Basic physical properties of the interior models of the planet hosts TOI-2018 and HD 155358, known for their very low surface metallicities. Surface abundances Z_s are derived from spectroscopic [M/H] and [α/Fe] measurements and are found to be 0.006 and 0.004, respectively. For both stars, the models converge to an initial heavy-element abundance $Z_0 = 0.007$, consistent with the minimum metallicity inferred for the 127 solar-like oscillating planet hosts.

Host	$T_{\rm eff}$ (K)	M $M_\odot$	R $R_\odot$	L $L_\odot$	t_9 Gyr	Z_0	Y_0	α	Z_s
TOI-2018	4306	0.57	0.57	0.10	10.50	0.007	0.2611	1.8311	0.006
Obs	4302	–	–	0.10	–	–	–	–	0.006
HD 155358	5954	0.96	1.33	2.01	7.23	0.007	0.2611	1.3035	0.004
Obs	5958	–	–	1.99	–	–	–	–	0.004

APPENDIX C: COMPARISON OF REVISED MASS AND RADIUS OF PLANETS AND HOSTS

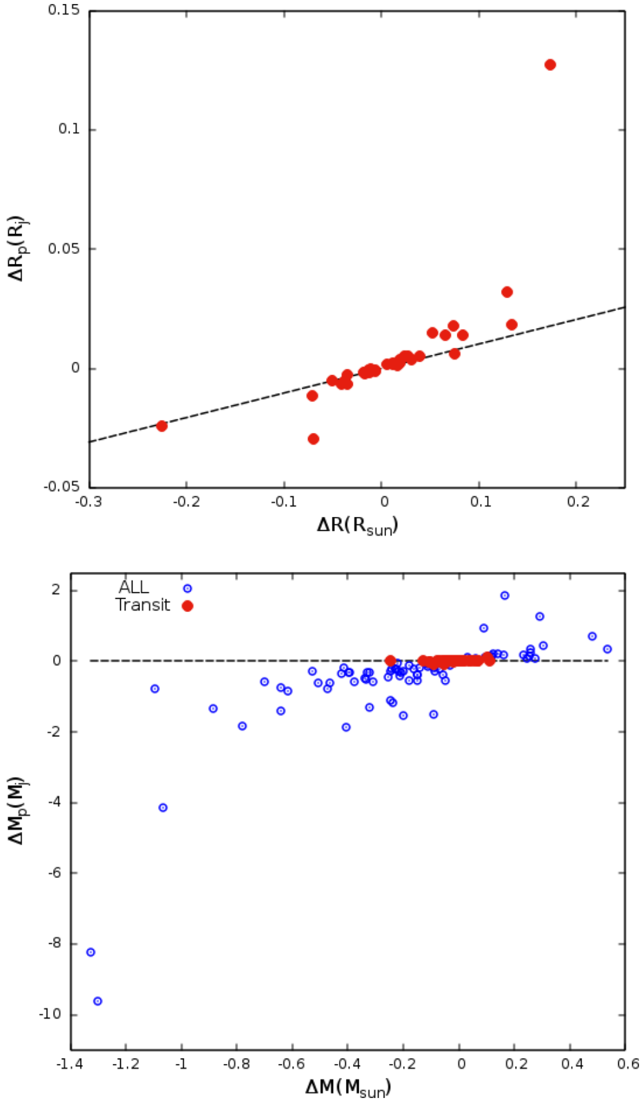

Figure C1. (a) The difference between $R_{\rm p}$ and $R'_{\rm p}$ is plotted with respect to R and R'. (b) The difference between $M_{\rm p}$ and $M'_{\rm p}$ is plotted with respect to M and M'.

This paper has been typeset from a TEX/LATEX file prepared by the author.